Urban Climate 68 (2026) 103049

Contents lists available at ScienceDirect

Urban Climate

journal homepage: www.elsevier.com/locate/uclim

Effect of street trees on turbulent exchange processes and flow circulation in urban street canyon: Application to air pollutant removal

Francesco Barbano [a,b,*], Erika Brattich [a], Silvana Di Sabatino [a]

[a] *Department of Physics and Astronomy "Augusto Righi", University of Bologna, Via Irnerio 46, Bologna, 40126, Italy*
[b] *Center Agriculture Food Environment (C3A), University of Trento, Via E. Mach 1, San Michele all'Adige, 38010, Italy*

ARTICLE INFO

Keywords:
Urban vegetation
Turbulent mixing
Pollutant dispersion
Street canyon
Ventilation

ABSTRACT

This paper investigates the role of trees in modulating the pollutant removal from a real urban street canyon. An integrated methodology is designed to incorporate the aerodynamic effect of trees in modulating the inertial and thermal forcing that drives the in-canyon circulation. Contextually, the efficacy of exchange processes in mixing momentum and heat is evaluated at different levels within and above the street canyon using time scales and their ratios. By linking the exchange process with the relative circulation, the impact on pollutant removal from the canyon is evaluated. Trees are found to sustain efficient momentum exchanges under inertial forcing as the production of turbulent momentum by the crown roughness and flow channelling in the trunk region generates fast mixing within the canyon. The faster mixing at the surface than at the canyon rooftop provides the ideal conditions for efficient momentum exchange between the canyon and the atmosphere above. Conversely, trees inhibit thermal mixing through the shading effect of their crowns, leading to inefficient exchange rates under thermal forcing. The pollutant concentrations follow inertial forcing, which favours pollutant removal from the canopy, and thermal forcing, which favours stagnation, revealing the benefits and drawbacks for air quality of a common tree deployment in the urban environment.

1. Introduction

Urban areas are the focal point of global aggregation owing to sustained urbanisation and population growth. At the same time, cities have become hotspots for climate change, exposing their inhabitants to a variety of environmental and health risks, mostly related to elevated temperatures (Piracha and Chaudhary, 2022; Brogno et al., 2025). Furthermore, inhabitants are constantly exposed to elevated levels of air pollution, which pose health risks (Kampa and Castanas, 2008; Piracha and Chaudhary, 2022) depending on factors such as the number and distribution of sources, city morphology, and local ventilation (Hankey and Marshall, 2017). Understanding the physical processes that characterise the urban boundary layer is paramount for delivering effective mitigation and adaptation measures to reduce inhabitants' exposure. At the local scale of the street canyon, key aspects such as flow circulations (Cheng et al., 2009; Cintolesi et al., 2021), coherent and transient turbulent structures (Zhang et al., 2022b,a), interaction and exchange processes (Chen et al., 2017; Barbano et al., 2021), and local thermal forcing (Nazarian et al., 2017, 2018) are responsible for the breathability (i.e., the ensemble of processes driving ventilation and pollutant removal, Buccolieri et al. 2010) and thermal comfort (Deng and Wong, 2020). As regulating mechanisms for city breathability, exchange processes

* Corresponding author at: Department of Physics and Astronomy "Augusto Righi", University of Bologna, Via Irnerio 46, Bologna, 40126, Italy.
E-mail address: francesco.barbano@unitn.it (F. Barbano).

https://doi.org/10.1016/j.uclim.2026.103049
Received 12 March 2026; Received in revised form 10 June 2026; Accepted 9 July 2026

Available online 1 August 2026

have been investigated as fundamental phenomena that drive the exchange of momentum and heat between the canopy and the atmosphere above through the rooftop interface (Bentham and Britter, 2003; Liu et al., 2005; Lo and Ngan, 2017; Barbano et al., 2020). Exchange processes are driven by the vertical fluxes of momentum (Louka et al., 1998; Kim and Baik, 2003; Barlow et al., 2004; Klein and Galvez, 2015) and heat (Nazarian et al., 2018; Barbano et al., 2021) at the rooftop interface, and their efficacy scales with the background wind speed (Harman et al., 2004), the turbulence kinetic energy transport (Salizzoni et al., 2011), and the thermal stratification (Nazarian et al., 2017) as well as the canyon aspect ratio (Barlow and Belcher, 2002) and rooftop geometry (Kastner-Klein et al., 2004). More recently, Barbano et al. (2021) highlighted the fundamental role of mixing at the pedestrian level of canyons with high aspect ratios ($H/W = 1.65$), where multiple vortices are likely to form. Specifically, effective ventilation for pollutant removal requires sustained mixing at the pedestrian level. Similar conclusions were drawn by Del Ponte et al. (2024) for a wide street canyon ($H/W = 0.5$) in the presence of trees, with their crowns hindering vertical transport.

In parallel, growing attention has been devoted to the use of green infrastructures (now included in the umbrella concept of nature-based solutions) in urban areas. The (dis)benefits of incorporating various vegetation elements into the complex texture of the urban canopy have been extensively investigated. Still, the debate remains open, especially when considering trees within a street canyon. Common investigations treat trees as porous obstacles that exert drag on the wind, favouring the absorption and deposition of atmospheric and soil compounds, supporting the urban water cycle, and shading canyon surfaces (Livesley et al., 2016; Salmond et al., 2016). Aerodynamic effects in particular provide competing results: to a typical net loss of momentum caused by a reduction in the wind speed (Buccolieri et al., 2011; Di Sabatino et al., 2015), turbulence production and dissipation can both increase in different regions of the canopy (Giometto et al., 2017; Santiago et al., 2019; Barbano et al., 2020; Fellini et al., 2022; Del Ponte et al., 2024, 2025), leading to uncertain conclusions on turbulent transport and mixing. Impacts on pollutant concentrations are also debated, with aerodynamic effects being a major factor in dispersion (Gromke et al., 2008; Buccolieri et al., 2009). On the other hand, air cooling is widely observed, especially in combination with other green infrastructures (Che and Zhuang, 2025), but the combined thermal-aerodynamic effects on ventilation remain unsolved (Cui et al., 2026). In these terms, city resilience becomes an evidence-based planning for the distribution, configuration, and selection of optimal vegetation species to maximise benefits for the urban atmosphere (Abhijith et al., 2017; Ullah et al., 2025; Li et al., 2025).

In this paper, we aim to expand on the work of Barbano et al. (2021) by investigating the role of exchange processes at different elevations within a street canyon, in the presence of vegetation, and their impacts on air-pollution removal. The investigation accounts for both inertial and thermal forcing of the in-canyon circulation and for turbulent processes that drive momentum and heat exchanges. To achieve this goal, the buoyancy parameter introduced by Dallman et al. (2014) to discern inertial and thermal forcing on the in-canyon circulation is modified to account for the aerodynamic effect of vegetation on the wind. A case study from a customised experimental field campaign provides a testbed for the investigation. Below, Section 2 delineates the methodology for the current investigation, Section 3 describes the field experiment and the dataset used for the analysis and discussion presented in Sections 4 and 5, respectively. Section 6 draws the conclusion.

2. Methodology

2.1. Inertial and thermal circulations in the presence of vegetation

Under weak synoptic forcing, the in-canyon circulation is known to be driven by inertial and thermal forcing, either exclusively or in mutual interaction. Specifically, when the background flow above the canyon top u_0 is sufficiently small, and the canyon walls are differentially heated, the thermal-driven circulation is supposed to prevail; conversely, the background flow inertia drives the circulation (Fig. 1). Following Dallman et al. (2014) conceptual scheme for a bidimensional circulation in a skimming flow regime, a dimensional analysis of the continuity equation implies that the cross-canyon and vertical velocity components relate through the mean canyon height H and width W so that $u/W + w/H \simeq 0$ for both inertial and thermal circulations. Under inertial forcing, the in-canyon velocity scales directly with the background velocity, as modulated by the aspect ratio $AR = H/W$. Instead, the thermal circulation velocity $\boldsymbol{u}_t = (u_t, w_t)$ can be estimated using the vorticity $\boldsymbol{\omega}$ equation. Following Pope (2001), the vorticity equation reads

$$\underbrace{\frac{\partial \boldsymbol{\omega}}{\partial t}}_{I} + \underbrace{(\mathbf{u}\cdot\nabla)\,\boldsymbol{\omega}}_{II} = \underbrace{(\boldsymbol{\omega}\cdot\nabla)\,\mathbf{u}}_{III} - \underbrace{\boldsymbol{\omega}\,(\nabla\cdot\mathbf{u})}_{IV} - \underbrace{\frac{1}{\rho^2}\nabla\rho\times\nabla p}_{V} - \underbrace{\frac{1}{\rho^2}\nabla\rho\times\nabla\boldsymbol{\tau}}_{VI} - \underbrace{C_D\left(\nabla\alpha_v|\mathbf{u}|\right)\times\mathbf{u}}_{VII} - \underbrace{C_D\alpha_v|\mathbf{u}|\boldsymbol{\omega}}_{VIII} \tag{1}$$

where I is the tendency of the vorticity, II is the advection, III and IV describe the modification of vorticity due to vortex stretching, tilting and realignment, and flow convergence/divergence, V is the baroclinic term (with ρ the air density and p the air pressure), VI is the viscous shear stress (with $\boldsymbol{\tau}$ the shear stress), VII and VIII describe the vorticity modification due to the vegetation drag tilting and shear. Specifically, term VII represents the change in direction of vorticity caused by the variation in the bulk density (in terms of foliage area-to-volume ratio α_v) of vegetation, exerting a drag force (with C_D the drag coefficient) on the flow (Perez et al., 2025). Term VIII is the shear generation caused by the sinking of vorticity, given the vegetation drag (Perez et al., 2025). Both terms are driven by drag associated with vegetation foliage density, providing sources (tilting) and sinks (shear) of vorticity.

Considering a y-independent canopy, as we can achieve in the canyon centre far from the street intersections, the circulation can be traced back to the bidimensional vortex shown in Fig. 1 and the only non-null component of vorticity is ω_y. Under this assumption, and considering vegetation-induced flow stretching/tilting and divergence c.f. Section 5, terms III and IV are negligible. Assuming

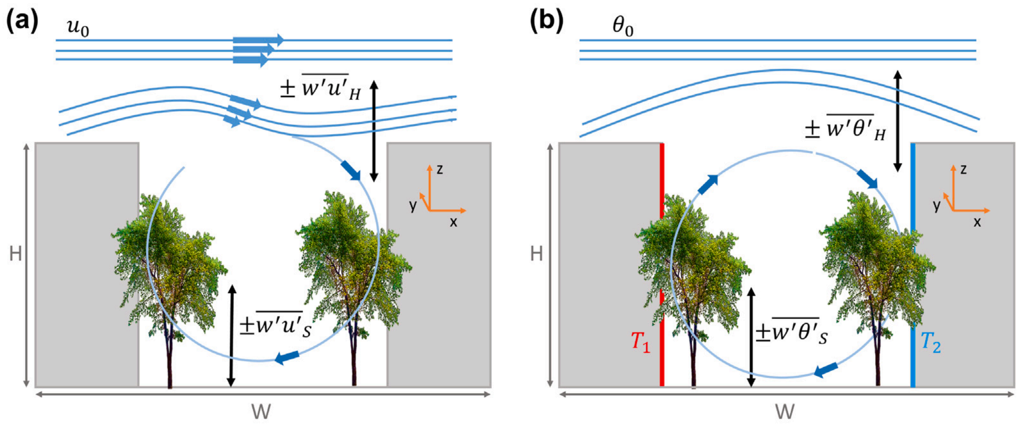

Fig. 1. Sketches of the inertial (**a**) and thermal (**b**) circulations. H and W are the mean canyon height and width, u_0 and θ_0 are the wind speed and potential temperature of the background flow, T_1 and T_2 are the surface temperature of the building facades, and $\overline{w'u'}$ and $\overline{w'\theta'}$ are the kinematic momentum and heat flux respectively at the canyon rooftop (subscript H) and pedestrian/surface level (subscript S).

quasi steady state and the Boussinesq approximation, also terms I and VI are neglected, while term V simplifies to the buoyancy b acting along the gravity direction; Eq. (1) can be simplified to evaluate the thermal circulation velocity, so that

$$\left(\boldsymbol{u_t} \cdot \nabla\right) \omega_y = \frac{1}{\rho^2} \nabla \rho \times \nabla p - C_D \left(\nabla \alpha_v |\boldsymbol{u_t}|\right) \times \boldsymbol{u_t} - C_D \alpha_v |\boldsymbol{u_t}| \omega_y, \tag{2}$$

with advection, baroclinic torque (buoyancy), and vegetation drag composing the balance. By applying dimensional considerations ($\nabla = (\partial/\partial x, 0, \partial/\partial z) = (1/W, 0, 1/H)$), recalling that $u_t/W + w_t/H \simeq 0$, and approximating α_v = LAD (Leaf Area Density), we can rewrite the along-canyon component of the vorticity as

$$\omega_y = \frac{u_t}{H} \left(1 + AR^2\right), \tag{3}$$

while the thermal circulation speed $|\mathbf{u_t}|$ becomes

$$|\boldsymbol{u_t}| = \sqrt{u_t^2 + w_t^2} = u_t \sqrt{1 + AR^2}. \tag{4}$$

Each term of Eq. (2) can be further approximated as follows.

Advection of vorticity

$$\left(\boldsymbol{u_t} \cdot \nabla\right) \omega_y \sim \left(\frac{u_t}{W} + \frac{w_t}{H}\right) \left(\frac{u_t}{H} \left(1 + AR^2\right)\right) = \frac{2u_t^2}{HW} \left(1 + AR^2\right); \tag{5}$$

Baroclinic torque

$$\frac{1}{\rho^2} \nabla \rho \times \nabla p \simeq \frac{1}{\rho_0^2} \nabla \rho \times \left(-\rho_0 g \hat{\mathbf{k}}\right) = \nabla b \times \hat{\mathbf{k}} \sim \frac{\partial b}{\partial x} = g\alpha \frac{\partial T}{\partial x} = \frac{g}{T_C} \frac{\Delta T}{W}, \tag{6}$$

where ρ_0 is the constant density within the canyon, g is the acceleration due to gravity, $\alpha = 1/T_C$ is the thermal expansion coefficient approximated with the mean air temperature within the canyon, and ΔT is the temperature difference between opposing building facades;

Drag tilting due to the vegetation

$$\begin{aligned} C_D \left(\nabla \alpha_v |\boldsymbol{u_t}|\right) \times \boldsymbol{u_t} &\sim C_D \left(\frac{\partial \mathrm{LAD}}{\partial z} u_t - \frac{\partial \mathrm{LAD}}{\partial x} w_t\right) |\boldsymbol{u_t}| \\ &= C_D \mathrm{LAD} \left(\frac{u_t}{H} - \frac{u_t H}{W^2}\right) u_t \left(1 + AR^2\right)^{1/2} \\ &= C_D \frac{\mathrm{LAD}}{H} u_t^2 \left(1 - AR^2\right) \left(1 + AR^2\right)^{1/2}, \end{aligned} \tag{7}$$

where the foliage drag and the aspect ratio of the canyon modulate the thermal circulation velocity, acting as a source of vorticity;

Drag shear due to the vegetation

$$C_D \alpha_v |\boldsymbol{u_t}| \omega_y \sim C_D \mathrm{LAD} u_t \left(1 + AR^2\right) \frac{u_t}{H} \left(1 + AR^2\right) = C_D \frac{\mathrm{LAD}}{H} u_t^2 \left(1 + AR^2\right)^{3/2}, \tag{8}$$

where the foliage drag and the canyon aspect ratio modulate the thermal circulation velocity, acting as a vorticity sink.

Re-assembling Eq. (2) using (5), (6), (7), and (8) and solving for u_t, we obtain an approximated equation for the thermal circulation velocity within the canopy

$$u_t = \left[\frac{g}{T_C} \frac{\Delta T}{W} \left(\frac{2}{HW} \left(1 + AR^2\right) + C_D \frac{\text{LAD}}{H} \left((1 - AR^2)(1 + AR^2)^{1/2} + (1 + AR^2)^{3/2}\right) \right)^{-1} \right]^{1/2} . \tag{9}$$

Following the same concept of Dallman et al. (2014), when the background flow cannot be neglected, inertial and thermal forcing are mutually active within the canyon. To discern the prevailing forcing, u_t can be related to the background velocity u_0 to define the buoyancy parameter $B = u_t^2/u_0^2$

$$B = \underbrace{\frac{g}{T_C} \frac{\Delta T}{W}}_{I} \left(\underbrace{\frac{2u_0^2}{HW} \left(1 + AR^2\right)}_{II} + \underbrace{C_D \frac{\text{LAD}}{H}}_{III} u_0^2 \underbrace{\left((1 - AR^2)(1 + AR^2)^{1/2} + (1 + AR^2)^{3/2}\right)}_{IV} \right)^{-1} , \tag{10}$$

where term I and II are the buoyancy and advection (inertial) forcing driving the canopy circulation, term III is the drag exerted by the vegetation on the flow modulated by the bulk density of the vegetation element, and term IV is the geometrical parameter of the canyon. This bulk expression provides a rather simple formulation combining ambient and surface forcing of the in-canyon circulation with the geometric parameters and the drag force of the vegetated elements modulating the flow. Although it does not aim to capture all the intricacies of a turbulent flow, it enables one to discern the nature of the canopy flow, whether inertially or thermally driven, using only a few (mean) variables.

We can define a critical buoyancy parameter B_c to distinguish the in-canyon circulation as inertial ($B < B_c$) or thermal ($B > B_c$). Vegetation enhances the denominator of Eq. (10), favouring the formation of an inertial circulation with respect to the thermal. Two main reasons support this behaviour:

- Vegetation enhances the mechanical turbulence source and sink as the flow interacts with the crown and increases the wind speed in the trunk region due to the flow channelling and the Venturi effect resulting from the flow streamline displacement caused by the reduced air volume below the crown (as schematised in Miri and Webb 2022).
- The presence of vegetation limits the temperature difference between opposing building facades by shadowing the surfaces from direct solar radiation.

Note that in the absence of vegetation, $C_D = \text{LAD} = 0$ and Eqs. (9) and (10) fall back into the original definition by Dallman et al. (2014).

2.2. Mechanical and thermal scaling for the canopy circulation

To quantify the efficacy of mixing in a street canyon caused by mechanical and thermal processes, Barbano et al. (2021) derived a set of time scales and exchange rates to inspect the local exchange processes at different canyon heights. Time scales define the time required to generate mixing within different canyon layers through momentum and heat exchanges. The longer the time, the longer the turbulent exchanges will take. At the rooftop (H), i.e., the interface between the urban canopy and the unconstrained atmosphere aloft, the mechanical τ_d and thermal τ_h time scales estimate the required time to exchange momentum and heat between the canopy and the atmosphere above:

$$\tau_d^H = \frac{H^3}{\overline{w'u'}\mid_H W} \frac{\Delta U_0}{\Delta z}, \tag{11a}$$

$$\tau_h^H = \frac{H^3}{\overline{w'\theta'}\mid_H W} \frac{\Delta \theta_0}{\Delta z}, \tag{11b}$$

where $\overline{w'u'}\mid_H$ and $\overline{w'\theta'}\mid_H$ are the turbulent kinematic momentum and heat fluxes respectively inferring the local transport of momentum and heat through the rooftop interface, $\Delta U_0/\Delta z$ and $\Delta\theta_0/\Delta z$ are the background flow velocity and potential temperature gradient estimating the atmospheric stratification. Time scales increase with canyon height and thermal stratification, and decrease with canyon width and flux intensity.

Inside the canyon (S), time scales describe the required time to exchange fresh air coming from the rooftop interface with the stagnant air of the canyon

$$\tau_d^S = \frac{H^2 u_*^H}{\overline{w'u'}\mid_S W}, \tag{12a}$$

$$\tau_h^S = \frac{H^2 \theta_*^H}{\overline{w'\theta'}\mid_S W}, \tag{12b}$$

and they depend on the in-canyon mixing driven by kinematic momentum $\overline{w'u'}\mid_S$ and heat $\overline{w'\theta'}\mid_S$ fluxes within the canyon, and the inflow of fresh air through the rooftop interface due to the friction velocity $u_*^H = (\overline{w'u'}\mid_H^2 + \overline{w'v'}\mid_H^2)^{1/4} \approx \overline{w'u'}\mid_H^{1/2}$ and temperature scale $\theta_*^H = \overline{w'\theta'}\mid_H / u_*^H$ at the top of the canyon. Eqs. (12a) and (12b) infer that exchange processes within the canyon operate a fast air refreshing only if the inflow of fresh air from the rooftop is coupled by an equally or faster removal of stagnant air from the bottom of the canyon. To evaluate the relationship between rooftop and in-canyon time scales, exchange rates are then evaluated as time-scale ratios to estimate the efficacy of turbulent transport from the canopy to the atmosphere above. We define the mechanical and thermal exchange rates as η_d^{-1} and η_h^{-1}, respectively, where:

$$\eta_d = \frac{\tau_d^S}{\tau_d^H} = \frac{\overline{w'u'}\,|_H}{\overline{w'u'}\,|_S}\frac{u_*^H}{H}\frac{\Delta z}{\Delta U_0}, \tag{13a}$$

$$\eta_h = \frac{\tau_h^S}{\tau_h^H} = \frac{\overline{w'\theta'}\,|_H}{\overline{w'\theta'}\,|_S}\frac{\theta_*^H}{H}\frac{\Delta z}{\Delta \theta_0}. \tag{13b}$$

Compared to Barbano et al. (2021), we consider the reciprocal of the quantity $\eta_{d,h}$ as a measure of the exchange rate, since it brings a more intuitive consideration: by increasing the intensity of the rate of exchanges of momentum and heat (increasing $\eta_{d,h}^{-1}$), the efficacy of air removal from the canopy also increases. In the original framework of Barbano et al. (2021), these two quantities were inversely proportional, leading to counterintuitive relationships, especially when exchange processes are applied to air-pollutant removal from the canopy. The basic concepts around the $\eta_{d,h}$ remain the same. If $\eta_{d,h} \sim 1$, the exchange processes within the canyon and at the rooftop are equally efficient, the whole canopy is well mixed, and its properties are directly affected by the free atmosphere above. As $\eta_{d,h}$ deviates from unity, the intensity of exchange processes becomes vertically heterogeneous, favouring the formation of isolated turbulent structures, with different consequences for efficiency. When $\eta_{d,h}^{-1}$ is larger than 1, $\tau^H > \tau^S$ and the exchange processes are faster within the canopy compared to the rooftop, favouring the transport of momentum and heat from the canopy outwards through the rooftop level, promoting interaction with the free atmosphere, and inhibiting the recirculation. In this context, momentum and heat are more efficiently removed from the canopy and air within the canyon is efficiently mixed with fresh air from above. In contrast, when $\eta_{d,h}^{-1}$ is less than 1, $\tau^H < \tau^S$ and the efficiency of mixing within the canyon diminishes, resulting in air becoming confined within the canyon while recirculating fresh air at the rooftop. The exchange of momentum and heat occurs predominantly in the upper segment of the canopy; fresh air is not efficiently transported to the ground, where the canopy's stagnant air can recirculate for longer.

To link the circulation regime identified using Eq. (10) and the exchange processes developing, a simple assumption is made so that we can define a total exchange rate

$$\eta_t^{-1} = \begin{cases} \eta_d^{-1} & \text{if } B < B_c \\ \eta_h^{-1} & \text{if } B > B_c. \end{cases} \tag{14}$$

When the circulation is inertial, the mechanical exchange rate is expected to dominate mixing generation. Conversely, the thermal exchange rate is supposed to prevail during thermal-circulation regimes.

Fig. 2. Top (a) and frontal views from north (b) of Laura Bassi Street. Source: Google Earth.

3. Data and methods

3.1. Field campaign description

3.1.1. Geographical context of the target canyon

At the core of the present evaluation, high-frequency meteorological measurements were collected during an extensive field campaign from 7 August to 26 September 2017 within the city centre of Bologna (44° 29′N, 11° 20′E, 56 m above mean sea level), a medium-sized city located in northern Italy. The campaigns were designed to investigate the complex behaviour of both the mean flow and turbulent structures, as well as their connections to local air pollution, in two real urban street canyons. The selected sites, namely Marconi Street (MA) and Laura Bassi Street (LB), represent the morphologies of their respective neighbourhoods. The present paper focuses on LB, a two-lane 700-m-long road, surrounded by a non-regular display of private houses (2 floors) and apartments (3–5 floors), with a mean building height $H = 17$ m (Fig. 2). The presence of a private garden facing the street increases the mean canyon width to $W = 25$ m, yielding a mean aspect ratio $AR = 0.7$.[4] The road is flanked by two lines of deciduous trees belonging to the *Platanus Acerifolia Mil* family, a hybrid of *Platanus Orientalis* and *Platanus Occidentalis* types, widely found in urban European habitats. The average height of the branch-free trunk is 4 m, and the ellipsoidal-shaped crown extends up to a mean height $H_{tree} = 15$ m, with a minor radius of 5 m. Along the street, trunks are spaced approximately 8 m apart, allowing a small amount of crown superposition. Di Nicola et al. (2022) estimated a Leaf Area Index (LAI) of 7.1 $m^2\ m^{-2}$, which is computed by integrating the LAI in the crown region. A value of the LAD of 0.65 $m^2\ m^{-3}$ is computed by integrating the LAI in the crown region. Finally, a drag coefficient $C_D = 0.25$ is used as estimated by Barbano et al. (2020). LB is oriented along the north-south direction, with a displacement of 24° from north. As a residential area, the road is open to private vehicular traffic and to some minor bus routes.

3.1.2. The monitoring site and equipment

Fig. 3 displays the main monitoring sites along the street canyon, while Table 1 summarises the instrumentation deployed in each site. Supporting meteorological data were retrieved from the permanent meteorological stations of Viale Silvani and Asinelli Tower (see Table 1) of the Emilia-Romagna Environmental Protection Agency (ARPAE) network to compute the background flow at the city scale. Further details on the experimental design and data collection, as well as additional materials on the instrumental equipment, can be found in Barbano et al. (2020, 2021).

Fig. 3. Monitoring sites in LB. Source: Google Earth.

For this work, a suitable dataset of four days (20–23 September) was selected to meet the requirement of weak-synoptic forcing. This condition enables the local circulation to dominate the small-scale dynamics (see Barbano et al. 2021 for the details on the period selection). Additionally, infrared images collected with a thermal camera (FLIR T620, FLIR Systems Inc., Wilsonville, OR, USA) at the same site but during a different period (i.e., 22–23 August) were used to examine the shadowing effect on the in-canyon surfaces. Among the 24-hour thermal campaign with infrared photographs collected every two hours (see details in Di Sabatino et al. 2020), the morning period (0700–1300 local time) is used for the current scope, and an east-facing building is analysed together with the street surface. Given the time discrepancy of the thermal campaign, the infrared photographs are used exclusively for a qualitative illustration of the shading mechanism provided by trees. No direct implications or quantitative relationships with the exchange processes (which are based entirely on the September dataset) will be made. Specific settings and parameters for the infrared data collection are listed in Appendix 1.

[4] The geometrical information on building elements has been computed in Barbano et al. (2020) from georeferenced regional databases using the QGIS software.

Table 1
Instrumentation set-up, sample rate, relevant measurements and uses of the collected data for the current study.

Experimental setup and measurements			
Station	Instrumentation	Sampling	Measurements
Rooftop level, LB3 (20 m a.g.l.)	Sonic anemometer 81 000, RM Young Company, Traverse City, Michigan, USA	10 Hz	Wind velocity sonic temperature
Mid-canyon level, LB2 (9 m a.g.l.)	Sonic anemometer Windmaster 3D, Gill, Lymington, Hampshire, UK	20 Hz	Wind velocity sonic temperature
	Thermohygrometer HCS2S3-L, Campbell Scientific, Logan, Utah, USA	1 Hz	Air temperature
Ground level, LB1 (3 m a.g.l.)	Sonic anemometer Windmaster 3D, Gill, Lymington, Hampshire, UK	20 Hz	Wind velocity sonic temperature
	Thermohygrometer HCS2S3-L, Campbell Scientific, Logan, Utah, USA	1 Hz	Air temperature
	Gas analyser T300, Teledyne API, San Diego, California, USA	1 min (average)	Carbon monoxide concentration
Silvani Street, SI (35 m a.g.l.)	Cup and vane anemometer WMS301, Vaisala, Helsinki, Finland	30 min (average)	Wind speed and direction
	Thermohygrometer HMP230, Vaisala, Helsinki, Finland	30 min (average)	Air temperature
Asinelli tower, AT (90 m a.g.l.)	Cup and vane anemometer Vv20 & Dv20, CAE, Bologna, Italy	60 min (average)	Wind speed and direction
	Thermohygrometer THS, CAE, Bologna, Italy	60 min (average)	Air temperature

3.2. Data processing

3.2.1. Despiking and rotation

The initial stage of data processing involved inspecting the dataset to identify and remove any non-physical values or instrumental failures. The criteria for data removal were based on typical local ranges: wind velocity components $|(u, v, w)|$ were limited to less than 20 m s^{-1}, air temperature $|T|$ was constrained to less than 50 °C. Values exceeding these thresholds were replaced with the nearest finite value from the time series. Sonic data were then despiked using a method similar to that of Højstrup (1993), which assumes that each 30-min data subset of the entire time series is independent and follows a Gaussian distribution. Values beyond a threshold $C \cdot \sigma$ (with σ being the standard deviation of the distribution and $C = 3.5$ according to Vickers and Mahrt 1997, Schmid et al. 2000) were marked as spikes. The despiking procedure is applied once per interval, replacing spikes with the mean calculated without them. After despiking, horizontal wind components were rotated according to McMillen (1988) to align with the streamline. Subsequently, all relevant quantities for this paper were averaged over 5-minute intervals. Different averaging periods were tested, and a 5-minute interval was selected as the best compromise between a robust representation of the mean quantities and a preservation of short turbulence fluctuations. An autocorrelation test was also performed, revealing that only air temperature is autocorrelated for more than 5 min, as expected and deemed acceptable given this variable's slow response in the absence of external perturbations. Finally, if erroneous values exceeded 50% within the 5-minute averaging period, those intervals were rejected. The data analysis is performed using customised MATLAB codes.

3.2.2. A brief note on traffic-induced momentum and turbulence

Vehicle traffic is not only a source of air pollutants, but it can also contribute to a local modification of momentum and turbulence intensity. Isolating traffic-induced contributions is important for reconstructing the components of the airflow and turbulence structures near the surface that are only affected by geometric and meteorological parameters, but it is not always straightforward, given the involved spatial and temporal scales. Considering the spatial scales, Cai et al. (2020) found that the area affected by the vehicle is confined to the immediate wake, with negligible effects in the perpendicular direction to the car's moving axis; Alonso-Estébanez et al. (2012) observed that disturbances decrease rapidly with height above the vehicle, especially for passenger cars. Considering temporal scales, Rao et al. (1979) identified the characteristic frequencies of traffic-induced turbulence in the range 0.1–1 Hz, but more recent observations have shown a wider spread towards lower frequencies (Gordon et al., 2012).

Given our instrumental setup, it is unlikely the vehicle wake extends to LB1, since it is located at a 3-m height and approximately 3–4 car widths aside the car lane. Moreover, given the imprecise identification of the characteristic frequencies and the possible overlap with the inertial subrange (Nelson et al., 2007), traffic-induced contributions are hard to isolate and remove. The bulk formulation of Di Sabatino et al. (2003) is used as a countercheck of the traffic-induced turbulence kinetic energy (TKE) in a 3.5 m layer above the street. Considering real traffic counts and assuming a single car model (an SUV to maximise the wake dimension) moving at a speed of 19 km/h (vehicle speed limit in the street is 30 km/h), the generated TKE is on average 5% (with peaks at 8%) of the measured value of TKE at LB1 during daytime, while it is negligible during the night. Assuming the same percentage for the momentum flux, the modes of time scales and exchange rates without the traffic-induced turbulence are modified by less than 5% of the values in the manuscript. For these reasons, we have chosen not to filter out traffic contributions, as any attempted filter would risk removing physically relevant atmospheric turbulence while failing to reliably isolate the vehicle signal.

3.2.3. Pollutant source and normalisation

To minimise the impact of additional sources other than traffic, we used carbon monoxide (CO) as a local passive tracer for the current analysis. Concentrations of CO were sampled at ground level within the canyon and normalised to the emission rate computed from vehicle counts and fleet disaggregation. This approach enables the minimisation of the source contribution to the measured pollutant concentrations and facilitates direct comparison with the exchange processes that are assumed to regulate pollutant ventilation (Murena and Favale, 2007). To derive traffic-related emissions, the approach developed by Barbano et al. (2021) is followed: buses were separated from the vehicle fleet, and the latter was further disaggregated by engine type and EURO technology. Bus counts were obtained from the bus schedule from the transportation agency operating in Bologna.[5] Vehicle counts were obtained using inductive loop technology at the city's principal traffic junctions. The fleet composition is extracted from the open data of the Italian Car Club (ACI).[6] Pollutant emission rates (g km^{-1}) are then estimated using the European Monitoring and Evaluation Program of the European Environment Agency (EMEP/EEA) air pollutant emission inventory for each vehicle category (European Environment Agency, 2016), and converted in pollutant emission source rate Q_e (g s^{-1}) using a representative vehicle urban speed of 19 km h^{-1} (European Environment Agency, 2016). Finally, the normalising factor CO_0 is computed as:

$$CO_0 = \frac{Q_e}{HWU_H}, \tag{15}$$

where Q_e is the pollutant source rate, U_{LB3} is the wind speed measured at the canyon rooftop modulating the mean-flow ventilation, H is the mean building height, and W is the mean street width that accounts for the geometric boundaries of the canyon.

The normalised concentrations CO^+ are retrieved by dividing the measured concentrations of CO by Eq. (15), and their distribution is plotted in Fig. 4.

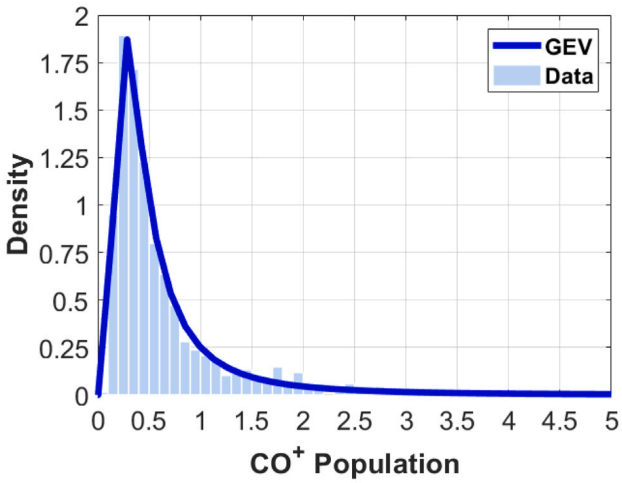

Fig. 4. Histogram and relative fit for the normalised CO+ concentrations computed from measurements collected in LB1 during the period 20–22 September 2017 (from 0000 of the first day to 12.30 of the last due to missing air pollution data from there to the end of the analysed period). Bin dimension is set to 0.1 units.

This quantity depends only on the local circulation developing in the canyon and the prevailing turbulent processes. In other words, this assumes mass transport to behave similarly to momentum and heat transport; therefore, CO^+ concentrations are expected to behave in opposition to the total exchange rate η_t^{-1}, which is a measure of the efficacy of turbulent processes in ventilating the canyon. The more efficient the exchange processes are, the less the CO^+ concentration will be. CO^+ concentrations can be properly fitted by the generalised extreme value (GEV) function. As we will show in Section 4.3, time scales and exchange rates will also follow the same distribution, validating the dependence hypothesis.

[5] https://www.tper.it/.
[6] http://www.aci.it/laci/studi-e-ricerche/dati-e-statistiche/open-data.html.

3.2.4. On the computation of the in-canyon temperature difference

The experimental design precludes a direct measurement of the air temperature near the opposing building facades. An indirect method is therefore adopted, following the modification introduced by Barbano et al. (2021) to the mean canyon temperature parametrisation defined by Solazzo and Britter (2007). Specifically, the mean temperature difference between opposing building facades within the canyon can be computed as

$$\Delta T = \left(2R\frac{H}{W} - 2\right)\left(T_1 - T_a\right), \tag{16}$$

where $R = (T_C - T_a)/(T_1 - T_a)$ is a constant retrieved from the mean canyon temperature T_C, the ambient temperature outside the canyon T_a and the temperature at one side of the canyon T_1. For the current case study, T_C is computed as the average temperature between values measured in LB1 and LB2, $T_a = T_{SI}$, and $T_1 = T_{LB1}$. Fig. 5 shows the distribution of the components of R.

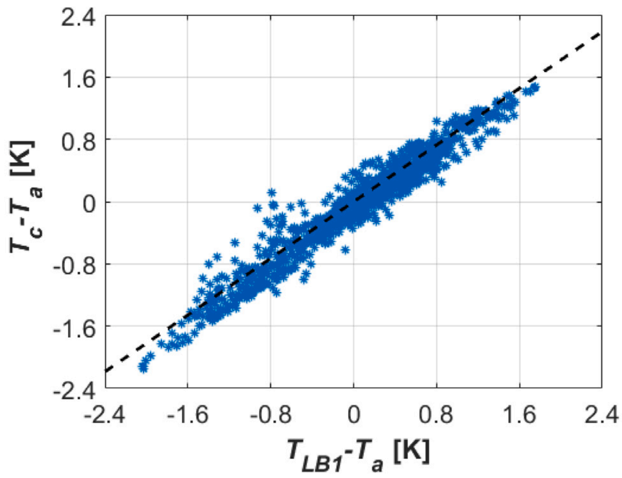

Fig. 5. Retrieval of the parameter R of Eq. (16) as the best linear fit ($Y = 0.91X$, in black) of the distribution.

From the best fit to the distribution, we retrieved the adopted value of $R = 0.91$ with high accuracy (coefficient of determination $R^2 = 0.93$, root mean square error RMSE = 0.18). Compared to Solazzo and Britter (2007), the value of R for the current case study is one order of magnitude larger. Nonetheless, one main difference must be considered: the street canyon in the literature was devoid of vegetation on both sides of the street, thereby altering the heating footprint of solar radiation on the buildings and the resulting thermal emission. The presence of vegetation, in turn, requires an independent computation of the heat forcing from the facades, which is modulated by tree shadowing. For this reason and the good scores obtained from the fit, we consider the estimation of R accurate for the current case study.

4. Results

4.1. Overview of the atmospheric characteristics

Atmospheric processes within the urban canyons are typically linked to the dynamics of the background flow at the urban scale and the thermal stratification of the urban boundary layer. Fig. 6 offers an insight into the wind speed and direction, and air temperature at different heights above the canopy, from the rooftop site in LB to the upmost weather station in AT.

Regardless of the intensity of the wind speed at AT and SI, the wind speed at the interface with the canopy remains smaller than 5 m s^{-1}. Velocity minima are observed at the transition between day and night, resulting in nearly calm conditions along the air column. Other wind speed values below 1 m s^{-1} are spread over the analysed period, favouring the development of a thermal circulation within the canyon. Wind directions exhibit a regular evolution over the period, alternating south-westerly flows at night to north-westerly–north-easterly flows during the day. The observed directions correspond to downslope/downvalley at night and upslope/upvalley during the day, suggesting that the background flow is affected by the slope/valley circulation developing along the southern hill chain leading to the city. Air temperature (missing in LB3, as only the sonic temperature was available at the site) shows the typical evolution under clear-sky conditions, with daytime values verging on vertical mixing and nighttime values characterised by inverse stratification. No trend is observed during the analysed period.

To further detail the wind field under (quasi)-stationary wind directions, profiles of the wind speed at key hours of the day and night are computed and shown in Fig. 7, including the canopy. Within the canopy, wind speed is largely homogeneous at night and during the day, increasing towards the rooftop. Above the canopy, similar wind speeds are measured at LB3 and SI, as mixing induced by convection dominates the diurnal wind profile in the roughness sublayer. During nighttime, a consistent wind stratification is observed above the canopy. The persistence of the background wind favours the development of the inertial circulation within the canopy sustained by turbulent momentum fluxes. When the background wind is instead smaller than the thermal forcing within the

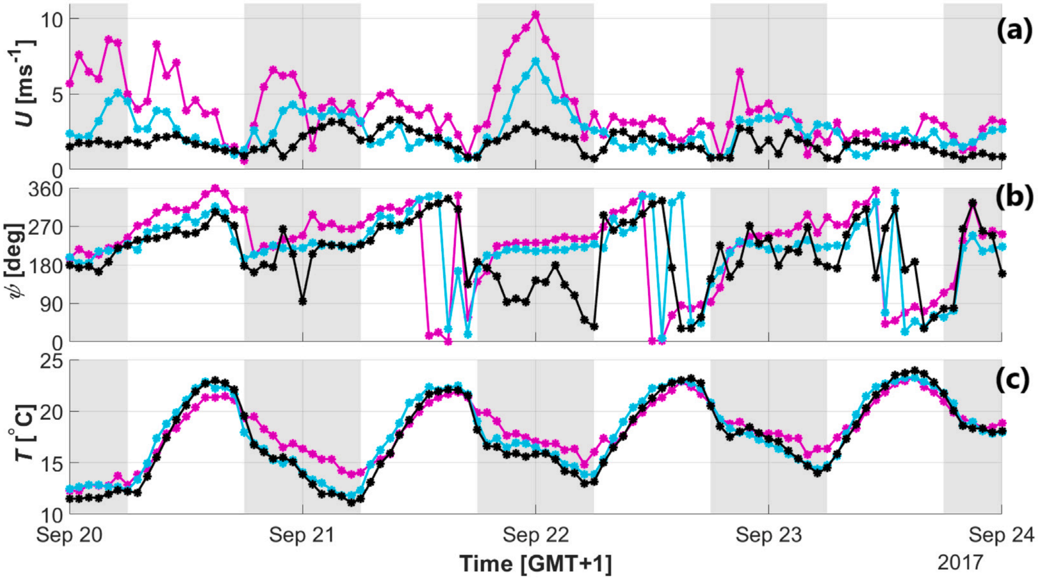

Fig. 6. Hourly mean wind speed **a**, wind direction **b** and air temperature c measured above the UCL. Colours indicate the following sites: magenta at AT, blue at SI, and black at LB3. The shadowed areas highlight nighttime periods. On average sun rises at 06:00 and sets at 18:00 (UTC+1).

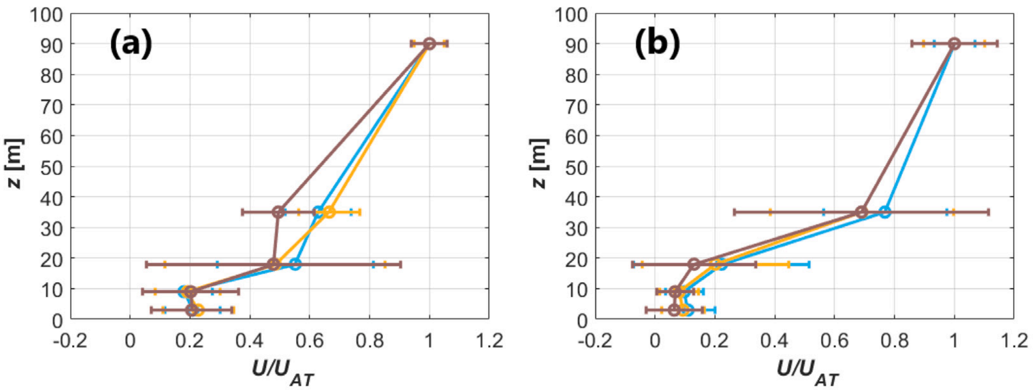

Fig. 7. Typical daytime **a** and nighttime **b** wind-speed profiles in Laurabassi Street coupled with SI referred to the period 20–23 September. Profiles are the hourly averages over the investigated period, taken at 12:00 (blue), 14:00 (yellow), and 16:00 (brown) UTC+1 during the day, and at 00:00 (blue), 02:00 (yellow), and 04:00 (brown) UTC+1 during the night. The normalising factor is the wind speed at AT for the same time intervals. The errorbars are the standard deviation of the mean.

canopy, the thermal circulation prevails, and the turbulent heat fluxes become the key parameter for the time scales. Fig. 8 displays the evolution of the turbulent kinematic momentum and heat fluxes at the three sites of LB. Momentum fluxes are constrained by the distribution and shape of buildings and trees, both of which increase the diurnal flux intensity compared to the rooftop level. Nocturnal hours show a smaller turbulence intensity, owing to the stratification of the background flow. Wind speed is also small within the canyon, where stratification is nearly negligible. Conversely, heat fluxes are smaller within the canopy as tree shadowing prevents a continuous heating of the street and facades, reducing the temperature difference between these surfaces and the air. During the night, fluxes remain small but mostly positive, as heat released from the surfaces sustains a continuous state of vertical mixing.

4.2. Circulation regime identification

The identification of circulation regimes and their link to exchange processes is evaluated for LB. Specifically, the ratio of the in-canyon and interface wind speed U_C/U_{LB3} is computed as a function of the buoyancy parameter B. When the circulation is

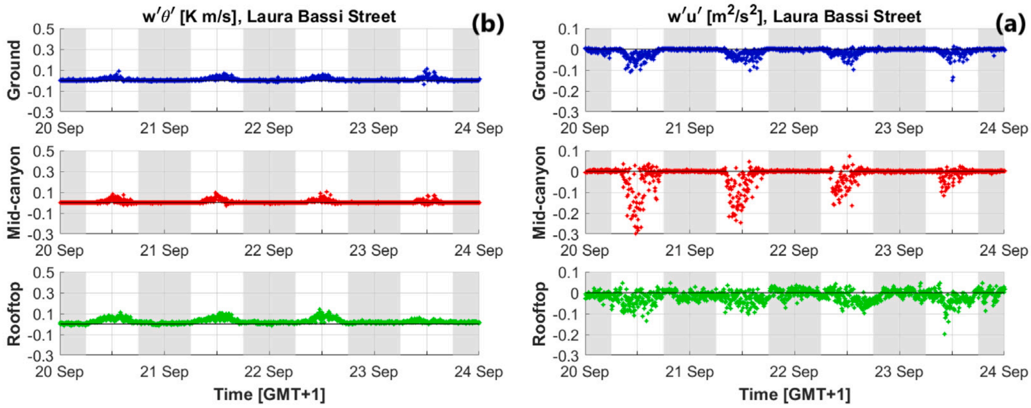

Fig. 8. Time evolution of the turbulent kinematic momentum **a** and heat **b** flux measured in Laurabassi Street during the period 20–23 September. Colours refer to ground (blue), mid-canyon (red) and rooftop (green) levels of the canyon, respectively. The shadowed areas highlight nighttime periods. On average, the sun rises at 06:00 and sets at 18:00 (UTC+1).

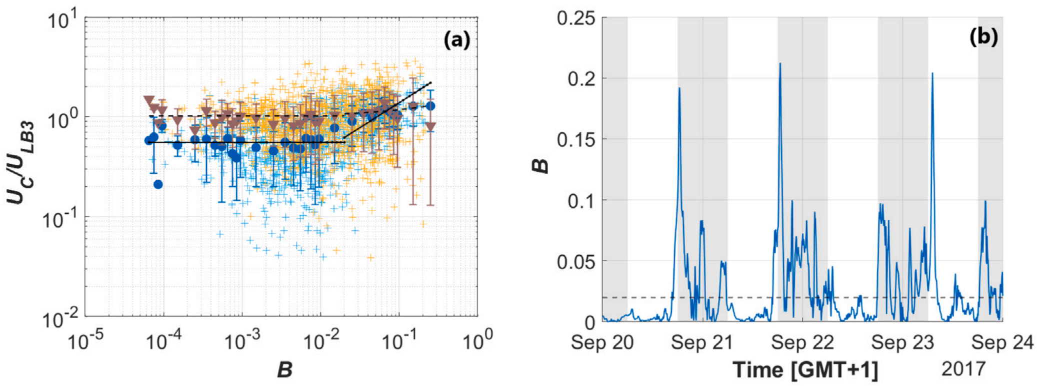

Fig. 9. **a** Wind speed ratios U_C/U_{LB3} as a function of B. Blue and brown cruxes are the 5-min-averaged ratios computed from LB2 and LB1 data. Blue (for LB2) and yellow (for LB1) full symbols are the bin-averaged ratios, and the errorbars represent the standard deviation computed in each bin. Dashed lines are the trends from which Eq. (17) is extrapolated, black for the one associated with the inertial circulation and red for the one associated with the thermal circulation. **b** Time evolution of the buoyancy parameter B. The dashed line identifies the critical values B_c. The shadowed areas highlight nighttime periods. On average sun rises at 6:00 and sets at 18:00 (UTC+1).

inertially driven, the in-canyon wind speed is expected to be proportional to the background wind speed arriving at the canyon rooftop, i.e., LB3. Conversely, when the circulation becomes thermally driven, the wind speed ratio must depend on B, which in turn depends on the circulation drivers, i.e., the horizontal temperature gradient between the opposite building facades. Dallman et al. (2014) proposed three simple trends for U_C/U_{LB3} depending on the circulation regime (inertial, thermal, and mixed) and a critical value B_c separating the inertially from the thermally/mixed driven: at $B < B_c$, the circulation is inertially driven and $U_C/U_{LB3} \sim C$ is a constant; at $B > B_c$, it can be thermal or mixed, both cases showing $U_C/U_{LB3} \sim B^{1/2}$. The critical value B_c separating the two regimes is empirically extracted from Fig. 9a upon fitting the expected trends as a piecewise function to the data; the optimal separation value B_c is obtained by minimising the root-mean-square error of the fits as the number of data points assigned to each regime systematically increased or decreased. Using this procedure, we obtained $B_c \simeq 0.02$, which is smaller than Dallman et al. (2014) and Barbano et al. (2021) as the presence of vegetation decreases the value of B with respect to a vegetation-free condition. This is consistent with a decrease in the wind speed ratio due to the flow deceleration induced by the tree crowns. LB1 shows a flatter distribution of the speed ratio with the buoyancy parameter than LB2, especially within the range of thermal circulation. This behaviour suggested the existence of two (or more) vortexes within the canyon, as typically observed under skimming flow regimes, possibly due to the geometrical configuration of the canyon (Zajic et al., 2011), the different tree drag with the elevation and channelling effect at the trunk level (Barbano et al., 2020; Cintolesi et al., 2023), or the opposing directions of buoyancy and inertial forces (Cintolesi et al., 2021). Wind channelling in the trunk region appears to be the most plausible effect in this case study, given the higher wind speed at LB1 than at LB2. The result is a mixed condition, where both mechanical and thermal forcing compete in driving the circulation characteristics in LB1.

The best fits retrieved from the distributions in Fig. 9a support the existence of a dual behaviour for the in-canyon thermal regime:

$$\frac{U_C}{U_{LB3}} \sim \begin{cases} C_1, & \text{if } B < B_c \\ C_2 \cdot B^{1/2}, & \text{if } B > B_c \text{ and } U_C = U_{LB2}, \\ C_3 \cdot B^{1/2} + C_4, & \text{if } B > B_c \text{ and } U_C = U_{LB1}, \end{cases} \tag{17}$$

where C_1 is 1.02 and 0.56 for LB1 and LB2, respectively, and $C_2 = 4.38$, $C_3 = 0.62$, and $C_4 = 0.98$. While LB2 shows an asymptotic form of $B^{1/2}$ for $B > B_c$, the ratio computed at LB1 is closer to a linear superposition of the supposed inertial and thermal regimes. As B grows larger than B_c, the wind-speed ratios computed with LB2 reach an asymptotic form of $B^{1/2}$, becoming larger than the ratios calculated using LB1. LB1 remains in a transition phase that extends into the supposed thermal regime, the pure form of which is not yet determined. As $B > B_c$, the tree crown sustains the circulation while the trunk modulates its intensity, preserving some inertial flow scaling. Another possible driver is the ground heating, which is not accounted for in the buoyancy parameter. In general, a transition phase between the two regimes is likely to exist, and the wind-speed ratio with LB2 can also be linearly fitted with reasonable accuracy, at least near B_c. At the same time, an asymptotic tendency is achieved at larger values of B.

Fig. 9b shows the evolution of B in time. At the transitions (sunset and sunrise), B attains its maximum value for the day as the canyon experiences differential heating across the opposing facades. During the daytime, the values of B are mostly below the critical value, with inertial forcing being the major driver. The thermal forcing prevails over the inertial forcing at sunrise and sunset, due to differential insolation of the east–west canyon facades, and at night, owing to heterogeneous temperature decay. Overall, thermal conditions are observed for 63% of the period, and inertial conditions for 37%.

4.3. Exchange processes in tailored circulation: Time scales and rates

4.3.1. Time scales evaluation

As defined in Section 2.2, time scales represent the amount of time required for an exchange process to develop. Time scales are computed at all levels within the canopies and at the rooftop to assess the different speeds of mechanical and thermal processes. The normalised density distribution of both time scales is shown in Fig. 10.

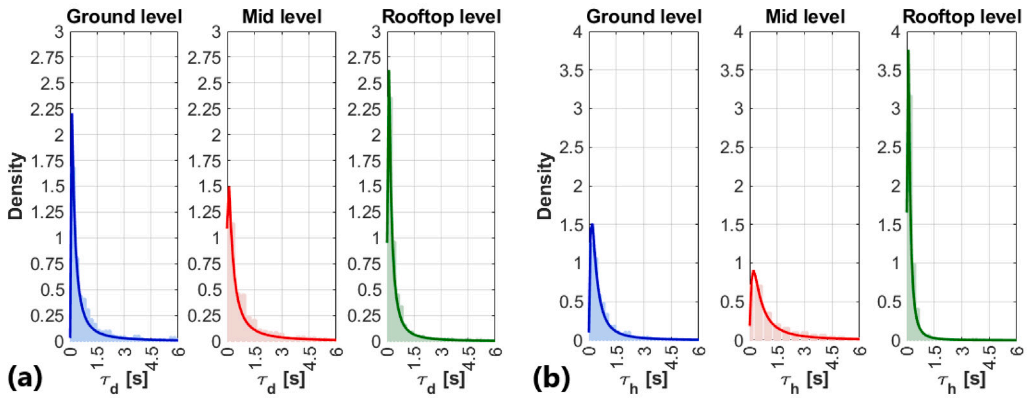

Fig. 10. Normalised density distributions of the 5-min average τ_d (a) and τ_h (b) data inside and above the street canyon during the analysed period (20–23 September 2017). Bin dimensions have been set to 300 s. Values of the abscissa are divided by 10^3.

The distributions have similar shapes, with modes in the first two bins and long directional tails in which occurrences rapidly decrease, suggesting mixing as the prevailing condition driven by large momentum and heat transports. Time scales increase when turbulent fluxes are suppressed or overpowered by larger-scale gradients. Exchange processes decrease their velocity almost monotonically and exponentially, but some extremely slow events have been detected, especially within the canopy. At the rooftop, both distributions have a steeper slope than those within the canyon, as mixed conditions can also be driven by small background flow gradients that reduce stratification and enhance vertical transport. Compared to the non-vegetated canopy in Barbano et al. (2021), the distributions are steeper and more strongly peaked on the modes, with a smaller occurrence of extremely slow events. The local atmospheric processes and site morphology favour rapid exchange processes by increasing overall turbulence intensity. This is particularly evident at the rooftop, where turbulent fluxes are enhanced by the additional crown roughness, which supports the turbulence production from the background flow (Barbano et al., 2020).

Following Barbano et al. (2021) and the evidence from Fig. 10, data distributions can be approximated through the GEV function, which is fitted to each distribution in Fig. 10 to retrieve the modes as an estimation of the more frequent, thus representative, value for the time scales as listed in Table 2. Goodness-of-fit metrics, including Akaike Information Criterion, Kolmogorov–Smirnov test, and Anderson–Darling test, support the use the GEV functions (see Appendix 2). The overall values of τ_d are more homogeneous than those of τ_h. At the ground level, the mechanical friction generated by surface roughness (Kastner-Klein and Rotach, 2004) is balanced by the flow acceleration due to lateral infiltration and channelling in the trunk region, thereby inducing a larger momentum

Table 2
Table summarising the characteristic time scales τ in LB derived from the modes of the probability density functions computed for the whole period (overall flow) and the background wind sectors from Table 3, where NP is north parallel, SP is south parallel, EWP is perpendicular (from east and west), and SW is southwestern. The error is estimated as 10% of the mode to account for the variability around the peak of the GEV distribution.

Laura Bassi Street time scales $\tau_{d,h}$ [s]						
	Level	Overall	NP	SP	EWP	SW
τ_d	Ground	100 ± 10	50 ± 5	210 ± 20	100 ± 10	110 ± 10
	Mid-canyon	110 ± 10	67 ± 7	200 ± 20	110 ± 10	210 ± 20
	Rooftop	110 ± 10	90 ± 9	100 ± 10	83 ± 8	110 ± 10
τ_h	Ground	160 ± 20	160 ± 20	180 ± 20	140 ± 10	210 ± 20
	Mid-canyon	210 ± 20	95 ± 10	370 ± 40	110 ± 10	310 ± 30
	Rooftop	100 ± 10	41 ± 4	80 ± 8	92 ± 9	89 ± 9

Table 3
Sectors for the discretisation in wind directions.

Sector colour	Sector name	Range
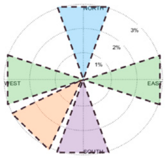	Overall	0°–360°
	South Parallel	160°–200°
	North Parallel	−20°–20°
	Perpendicular	70°–110° and 250°–290°
	Southwestern	205°–245°

flux. At mid-canyon and rooftop levels, the drag exerted by the tree crown sustains a moderate turbulence production, decreasing the modes of τ_d. τ_h varies between the levels above and inside the canyon, where they are also larger than τ_d. At the ground and mid-canyon levels, the thermal time scale is longer than the rooftop level, owing to the shadowing (cooling) effect of trees, which lowers the surface temperature and mitigates the heat release from the street (Li et al., 2012). At the rooftop level, the effect of vegetation is negligible, and the time scale is only modulated by the local heat flux and thermal stratification.

To further detail the exchange processes, the time scale computation is also performed after discriminating the data according to the wind direction classification in Table 3, with modes retrieved from the same data analysis of the overall time scales listed in Table 2 as well. The classification isolates sectors of the background wind direction that are parallel, perpendicular, or oblique (45°) to the canyon orientation. For the oblique sector, we only selected the southwestern wind direction, which corresponds to the typical wind direction in Bologna. Compared to the overall τ_d, the homogeneity retrieved for the specific wind sectors is mostly maintained within the canopy, while the rooftop is decoupled. When the background wind is parallel to the north, the air column is well mixed within the canyon by turbulent transport and heat released by the surfaces, while the rooftop is consistent with the overall value. This wind sector is the sole exception to the other directions, where the value of τ_d at the rooftop level is either equal to or smaller than that of the in-canyon. Although counterintuitive, the enhanced canopy roughness should increase the time scales, yet the north parallel condition is mostly transient and perturbed. τ_h under the north-parallel direction displays a similar behaviour to the overall condition. Modes retrieved under south-parallel and southwestern wind conditions show the largest values of τ_d and τ_h among the different wind direction cases, corresponding to small momentum and heat fluxes, especially within the canyon, where the tree drag is observed to reduce the turbulence intensity (Del Ponte et al., 2025) and the crown shadowing is effective. A certain difference is also evident in τ_d and τ_h for the perpendicular background wind direction. Mechanical time scales are shorter at the rooftop, while roughness remains effective in inhibiting the momentum flux within the canyon, thereby enhancing τ_d. τ_h is again homogeneous inside the canyon and faster at the rooftop level, owing to the shadowing effects of trees on the in-canyon surfaces. The results for the perpendicular case are in line with Zhao et al. (2023) when considering large trees.

Compared to Barbano et al. (2021), the mechanical and thermal time scales are smaller both within and above the canopy. Different aspects may underlie the differences between these two studies.

Aspect ratio: Despite the canyons from both studies being associated with the skimming flow regime, the wider-than-higher canopy of this study enables more effective flow circulation in the canyon, favouring the momentum, heat, and mass exchanges.

Vegetation: The presence of trees introduces physical boundaries that can modify the effective aspect ratio of the street, decreasing the air volume of the canyon. Moreover, the crown drag and the flow acceleration in the trunk region can alter the momentum transport (increasing or decreasing it). In contrast, the crown shadowing reduces the heat flux from the surface.

Morphology: The presence of irregular and spaced buildings favours the lateral flow infiltration in the street, enhancing the ventilation and favouring the air recirculation, lowering the time scale.

Disentangling these contributions is not feasible in the current experimental setting, but we believe they are all contributing factors in ultimately lowering the value of time scales relative to a more densely built, non-vegetated canopy.

4.3.2. Exchange rates evaluation

Eqs. (13a) and (13b) characterise the rates of turbulent mixing and transport of atmospheric particles within the canyon, distinguishing between mechanical and thermal processes. From a practical standpoint, the exchange rates are referenced to ground level when ratios are computed using the time scales at the rooftop and ground levels, and to the mid-canyon level when the ratios incorporate time scales from both the rooftop and mid-canyon levels. The results have then been classified based on the wind-direction sectors defined in Table 3. GEV functions are then fitted to the distributions in a manner consistent with the approach applied to the time scales (see Appendix 2 for goodness-of-fit metrics). The modes of the GEV functions are reported in Table 4.

Table 4
Table summarising the characteristic exchange rates η in LB derived from the modes of the probability density functions computed for the whole period (overall flow) and the background wind sectors from Table 3, where NP is north parallel, SP is south parallel, EWP is perpendicular (from east and west), and SW is southwestern. The error is estimated as 10% of the mode to account for the variability around the peak of the GEV distribution.

Laura Bassi Street exchange rates $\eta^{-1}_{d,h}$						
	Level	Overall	NP	SP	EWP	SW
η_d	Ground	3.6 ± 0.4	5.0 ± 0.5	9.1 ± 0.9	6.3 ± 0.6	5.0 ± 0.5
	Mid-canyon	2.6 ± 0.3	0.10 ± 0.01	6.7 ± 0.7	6.3 ± 0.6	6.7 ± 0.7
η_h	Ground	1.0 ± 0.1	0.14 ± 0.01	0.56 ± 0.06	0.83 ± 0.08	0.63 ± 0.06
	Mid-canyon	0.56 ± 0.06	0.13 ± 0.01	0.50 ± 0.05	0.67 ± 0.07	0.32 ± 0.03

Mechanical exchange rates are found to be efficient regardless of the background wind direction. Mechanisms regulating turbulent transport of momentum within the canopy are faster than at the rooftop, inducing an efficient ventilation of the lower levels of the canyon. The most advantageous condition for efficient exchanges throughout the canopy is found under south-parallel wind direction, when the channelling effect of wind is likely to favour this ventilation. Under thermal forcing, the probability of having stagnant conditions within the canopy increases as $\eta_h^{-1} < 1$. The heat flux is typically larger at the rooftop while being mitigated by the shadowing effect of trees, which partially shields in-canyon surfaces from direct solar radiation. As a consequence, disadvantageous conditions are established, and exchange processes are strongly inhibited regardless of the background wind direction.

4.3.3. Comparison between the exchange rates and the normalised pollutant concentrations

The total exchange rate η_t^{-1} defined in Eq. (14) is compared with the normalised CO concentrations to infer its efficacy in removing the pollutant from the canopy depending on the circulation and the background wind direction.

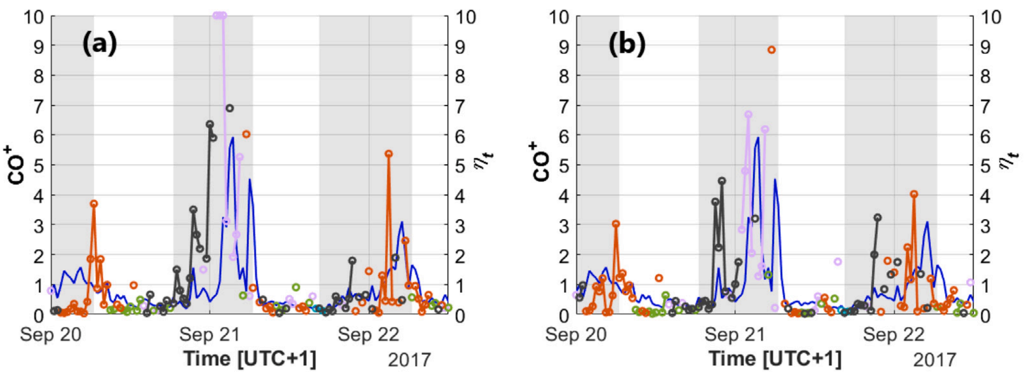

Fig. 11. Comparison between the normalised concentration CO^+ and the reciprocal of the total exchange rate η_t for **a** the rooftop to ground level and **b** the rooftop to mid-canyon level exchange rates. The continuous blue line refers to the CO^+ concentration; coloured lines with markers refer to η_t following the wind-direction classification (north parallel displayed in light blue, south parallel in purple, perpendicular in green, south-west in orange, and the remaining sectors in black). The shadowed areas highlight nighttime periods. On average sun rises at 06:00 and sets at 18:00 (UTC+1).

To avoid capturing sudden variations in the exchange rate and focus on the bulk evolution of its signal compared to that of air pollution, both η_t^{-1} and CO^+ are further averaged over 30-min intervals. Fig. 11 shows the evolution of η_t compared to that of CO^+ concentrations in LB1 and LB2 after the discretisation wind-direction sectors (see Table 3). Regardless of the background wind direction, the exchange rate reciprocal η_t aligns with the evolution of CO^+ concentrations, especially during daytime. Therefore, as the intensity of the exchange rate η_t^{-1} grows larger, the concentration of CO^+ decreases as they are increasingly removed from the canyon. The enhanced turbulence activity favours an efficient mixing within the canyon, and CO^+ concentrations remain small. As the air within the canyon undertakes a faster mixing than the rooftop ($\eta_t < 1$), the pollutant emitted at the surface is diluted and transported away from pedestrians' heights, decreasing concentrations and exposure. During nighttime, concentrations increase following the decrease in the turbulence intensity and the increase in the atmospheric stratification above the canopy. The latter factor is particularly effective during the second night, when thermal stratification is enforced by a dynamic stratification, favouring the decoupling between the canopy and the atmosphere above and the trapping of scalars towards the surface, given the small turbulence transport. The η_t is consistently larger than 1 during the second night and shows peaks at specific times during the other two, capturing the overall evolution of CO^+ concentrations despite a tendency to overestimate and anticipate them. The rapid oscillation of the heat and momentum fluxes compared to a bulk quantity such as CO^+ can justify the larger oscillations in the evolution of the exchange rate. On the other hand, η_t anticipates any increase in the pollutant concentrations, probably because of a delay time between the establishment of the nocturnal regime and the impact it may have on CO^+ concentrations. Both factors are more evident with oblique wind directions to the canyon, when the in-canyon regime is mixed between the typical 2D vortex under perpendicular wind direction and the flow channelling of the parallel one (Zajic et al., 2011). Under south-parallel directions, the exchange efficacy is minimum, and CO^+ accumulates. It can be concluded that exchange processes developing as heat and momentum exchanges between the lower and upper parts of a canyon under inertial and thermal circulations, respectively, provide a direct and reliable approach to evaluate the variation of passive pollutant concentrations within an urban canopy with (and without) the presence of vegetation.

5. Discussion

5.1. Buoyancy parameter as a means to compare different street canyon flow characteristics

The buoyancy parameter defined by Dallman et al. (2014) and its modified version here derived to account for vegetation are simple, yet reliable quantities to discern the thermal and inertial contribution to the in-canyon circulation. Furthermore, Barbano et al. (2021) used it to compare the dynamics within street canyons of different aspect ratios. Using a bulk approach, both the parameter B and the velocity ratio u_C/u_{LB3} can be scaled to the target aspect ratio to obtain a bulk estimation of its behaviour. This approach relies on the dependence of the in-canyon dynamics (Oke, 1987; Soulhac et al., 2008) and temperature (Solazzo and Britter, 2007) on the aspect ratio, which can be used to scale both temperature difference (to then recompute B) and wind-speed ratio. Briefly, to rescale the wind-speed ratio, U_C/U_{LB3} is divided by the current aspect ratio and multiplied by that of the target canyon. To rescale the ΔT, the aspect ratio of the target canyon is inserted in Eq. (16). Fig. 12 compares the rescaled wind-speed ratio from this paper to the street canyon of Dallman et al. (2014) from the original experiment used to define B. To account for the missing vegetation in Dallman et al. (2014) canyon, C_D in Eq. (10) is set to zero when the value is rescaled. From the comparison, the scaled data are close to Dallman et al. (2014) despite the bulk approximation that accounts for the vegetation and the different building distribution. Vegetation alters the transition between inertial and thermal circulation regimes, favouring the inertial one thanks to the shadowing effect of the crowns, and driving a mixed circulation in the trunk region, where the reduced air volume of the canyon imposed by the trees dismantles the differences in the circulation regimes. The morphology of LB enables a horizontal flow infiltration between buildings that can favour the inertial circulation, changing the complexity of the environment and lowering the comparability. Both contributions are consistent with lower values of the wind-speed ratio U_C/U_{LB3} of the present case compared to that of Dallman et al. (2014), where the semi-idealised setup was aimed to reproduce a more ideal street canyon without obstacles within it. Considering the bulk nature of the rescaling approach, the comparison is satisfactory and can foster further investigations to refine the comparability of some thermodynamic characteristics of real street canyons with and without vegetation.

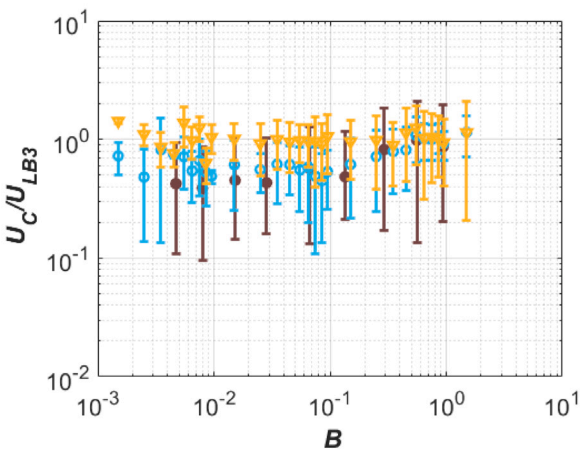

Fig. 12. Wind speed ratios U_C/U_{LB3} as a function of B. Blue (for LB2) and yellow (for LB1) symbols are the bin-averaged ratios with errorbars from Fig. 9 rescaled to compare with the full brown symbols retrieved from Dallman et al. (2014).

Finally, it is also worth noting that to the best of our knowledge, this is the first application of the buoyancy parameter B to a vegetated street canyon. Although the values of B_c are close to those Dallman et al. (2014) and Barbano et al. (2021) obtained for the non-vegetated canyon, a systematic assessment across different aspect ratios, tree species, and crown geometries is required before considering B_c a universal constant or establishing its dependence on geometrical parameters.

5.1.1. Varying vegetation characteristics in the buoyancy parameter

The aerodynamic characteristics of trees are typically summarised with key parameters, as we did for the drag coefficient C_D and the LAD. Also typical is the tendency to define these parameters as constants, depending on the tree species and dimension, especially when used in bulk formulations. Nonetheless, both C_D and LAD are functions of the elevation (crowns have a different drag than trunks, and foliage density changes within the crown) and season, other than the vegetation species and age. The adoption of constant values arises from the necessity to simplify the mathematical frameworks and the difficulties in measuring these parameters. The outcome is a large variability in the literature concerning the proper values to use, especially in numerical modelling. In its review paper, Goncalves et al. (2023) observed that typical values of C_D for trees in urban canopies (not single trees) range between 0.2 and 1.7 depending on the wind speed. To the best of our knowledge, there is no recent review paper reporting typical LAD values in urban environments, but upon a brief research, the commonly used LADs range between 0.3 and 2.5 $m^2\ m^{-3}$ (Lalic and Mihailovic, 2004; Jeanjean et al., 2015; Di Sabatino et al., 2015).

To evaluate the sensitivity of our study to the parameters defining the tree's characteristics, the buoyancy parameter B is calculated for several values of C_D and LAD in the previously found ranges. To avoid misleading contaminations, the atmospheric forcings u_0, T_C and ΔT are taken as constants computed as their respective average values during the investigated period, namely $u_0 = 1.6\ m\ s^{-1}$, $T_C = 291$ K and $\Delta T = 0.5$ °C. To evaluate the single contribution of the two parameters, C_D is set as a constant when LAD varies and vice versa. As constant values, we used $C_D = 0.25$ and LAD = 0.65 as in the rest of the paper.

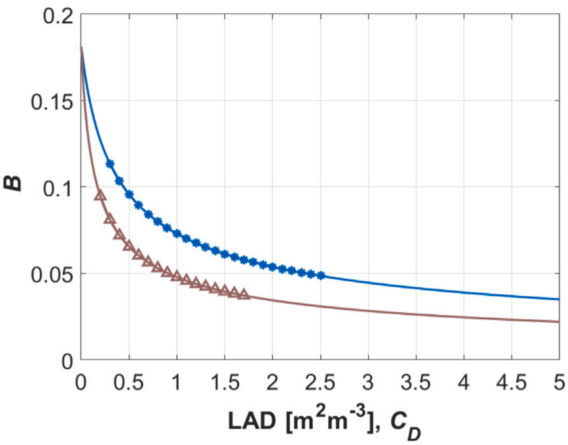

Fig. 13. LAD in blue, CD in brown.

Fig. 13 shows the variability of B with C_D and LAD. Both parameters have a similar impact on B, driving a steep decrease at C_D = LAD < 0.75 and a smooth convergence towards the respective asymptotic behaviours at higher values. In the typical ranges of the parameters, C_D and LAD are responsible for 32% and 36% of the variability of B for a given background wind and in-canyon thermal environment of this exercise considering the idealised condition $C_D = \mathrm{LAD} = [0, \infty]$. The percentages rise to 79% and 73% if we extend the typical ranges to C_D = LAD = 0, where B converges to 0.18, in line with the largest values detected in Fig. 9b and the role of trees in decreasing circulation speed within the canopy. It becomes clear that having precise information about the tree characteristics is mandatory even for bulk assessments of the urban canopy layer.

5.2. On the shadowing effect by the tree crown on the canyon surfaces

To further detail the shadowing effect of tree crowns on in-canyon surfaces, this section provides insights into the thermal properties of these surfaces. The sample surfaces are an east-facing building partially covered by a tree crown and a portion of the canyon street viewed from the north. Fig. 14 shows two sample infrared photographs collected during the investigation period. From each photograph, two portions of the target surface (boxes in Fig. 14) are identified as homogeneous areas irradiated from direct sunlight and covered by vegetation, from which the surface temperature is retrieved and analysed.

The portion of the target surface is arbitrarily selected, ensuring the homogeneity of the surface portion and the presence/absence of vegetation coverage. The first condition is imposed to ensure the emissivity of the surface remains constant, thereby preventing errors associated with its variability between different materials. Moreover, the surface is chosen so that the emissivity of each material is larger than 0.9 to minimise the reflected radiation.

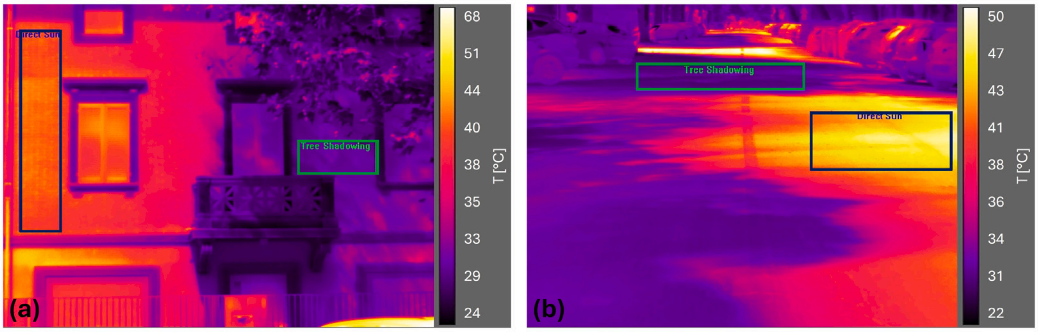

Fig. 14. Infrared photographs of the sample **a** building facade and **b** street in Laura Bassi Street, and arbitrarily identified surface portion under direct solar radiation (blue) and shadowed by the tree crowns (green) used to compute the time series in Fig. 15. The colorbar represents the surface temperature in Celsius degrees and is shown following the Plateau Equalisation[4] scale customised using the ResearchIR4 software of FLIR Systems. Photos are taken at 1100 and 1328 UTC+1, respectively. Details on the IR camera settings are listed in Appendix 1.

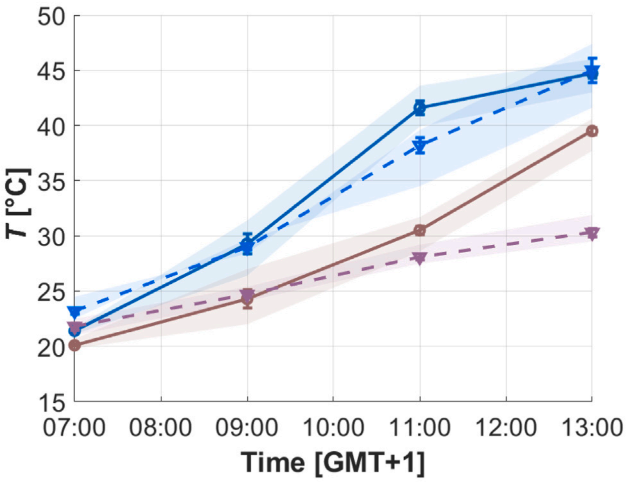

Fig. 15. Evolution of the mean surface temperature and standard deviation referring to the homogenous portion of target surfaces with and without shadowing from tree crowns. Symbols are the mean temperature value, bars are the standard deviation computed within the surface portion, and the coloured areas are the minimum–maximum range in the surface portion. Surfaces directly exposed to the sun are depicted in blue; those shadowed by the foliage are in red. Solid lines refer to the building facades, and dashed lines to the street pavement. Details on the IR camera settings are listed in Appendix 1.

Emissivity from each surface is obtained from online databases and verified in the field with an ad hoc procedure directly on the target surface. The thermal camera directly accounts for the radiative contribution from the atmosphere.

From each box in Fig. 14, the average surface temperature is retrieved from the photograph, together with the standard deviation and the temperature-range limits within the box. The analysis is performed through the IR Research software of FLIR System Inc. company and MATLAB coding. This operation is repeated on the same boxes from 0700 to 1300 local time, when the sunlight is direct towards the subject building, and the four time series of the surface temperatures (building and street under direct sunlight and covered by the tree crown) are displayed in Fig. 15. Unexpectedly, the temperature of surfaces directly exposed to solar radiation is higher than that of shadowed surfaces, with the difference increasing over the course of the day from sunrise to midday. The shadowing seems more effective on the street than on the building facade, as the latter received less effective coverage, especially in the late morning. The temperature difference between a shaded/non-shaded facade reaches 11.1 °C, while for the street it is 14.7 °C, with averages over the period of 5.7 °C and 7.6 °C, respectively, guaranteeing a consistent difference in the in-canyon thermal forcing.

[4] Non-linear, histogram-based algorithm. Provides good contrast for almost all scenes. The slider, next to the drop-down, controls the aggressiveness of the algorithm.

5.3. The role of trees in shaping the aspect ratio: what are the consequences for air pollution?

Another well-known effect of trees is that they enhance the canyon roughness, providing modification in the dynamics and turbulent transport (Barbano et al., 2020; Del Ponte et al., 2025) that causes alteration in the ventilation and pollutant dispersion (Nosek et al., 2016; Del Ponte et al., 2024), depending on the tree size and distribution (Moayedi and Hassanzadeh, 2022), the aspect ratio (Buccolieri et al., 2009) and background wind direction (Buccolieri et al., 2018), among other factors. The overall impact on the pollutant concentrations is still debated, but scenarios of increasing concentrations at the pedestrian level are documented (e.g., Di Sabatino et al. 2015), exposing the inhabitants.

Taking advantage of the experimental setup of this field campaign, we can compare MA and LB to argue about the effects of trees on air quality. Compared to LB, MA has a larger aspect ratio ($H/W = 1.65$), is more trafficked and is more densely built (see Barbano et al. 2021). The traffic rate is arguably the main source (at least during summertime) of CO and NO within the city centre: the average ratio of traffic counts between MA and LB is 1.64, discounting bus transits, which are again more abundant in MA. Together with the morphological disadvantage of MA, CO and NO concentrations are expected to be larger in MA than LB, but the ratios (LB/MA) are 0.95 and 1.17, respectively. The result is not sufficient to infer the negative role of trees in deteriorating the air quality at the pedestrian level, but it aligns with the results previously obtained throughout the current investigation. It also opens a debate on whether trees have to be included in the computation of the aspect ratio: their aerodynamic effect has a tangible impact on circulation and ventilation, to some extent similar to that of the building. Arguably, packed lines of trees on both sides of the street can form an effective, even if porous and heterogeneous, canyon with an aspect ratio H_{tree}/W_{tree}, with H_{tree} the mean tree height and W_{tree} the mean distance between opposing trunks or crowns. Under this assumption, the effective aspect ratio of LB would be $AR_{tree} = 1.36$, much closer to that of MA investigated in Barbano et al. (2021). Addressing and verifying this aspect is beyond the scope of this paper, but we hope it can lead to future investigations.

5.4. Theoretical assumptions and limitations

The theoretical model of the buoyancy parameter introduced in Section 2.1 is designed among a constraining set of assumptions that limit the strict application to real flows. Although the Boussinesq approximation can be achieved, especially at the spatial scales and small temperature differences of typical street canyons (see Dallman et al. 2014, Cintolesi et al. 2021), the bi-dimensional design is, in principle, less flexible. Indeed, this last constraint imposes that the background flow be perpendicular to the canyon, a condition that is, on the one hand, widely studied both experimentally and numerically, but, on the other hand, less common in reality, where winds are often deflected from perpendicularity. The in-canyon flows thus generated are therefore much more complex, displaying some helicoidal structures (see, for instance, Zajic et al. 2011) that reintroduce vorticity modification due to vortex stretching and give a 3-D shape to the turbulent flow, which becomes much more difficult to model in a theoretical, yet practical, framework. In addition, the drag force of leaves can promote the formation of small 3-D eddies, at least in the wake of the tree, where they can produce a modification of vorticity due to vortex stretching.

To preserve the practical use of the buoyancy parameter, simple considerations can be made. Away from major intersections, the in-canyon flow can develop in quasi-stationary structures that take the shape of circular or helical vortices, depending on the background wind direction and the portion of flow channelling under parallel directions. Sharing similar cross-sections, we can assume that these structures behave similarly to the idealised bi-dimensional canyon, to which we can trace back for a bulk inspection. The 3-D eddies generated by vegetation are expected to be (i) small in scale compared to that of the canopy circulation and (ii) confined to the vicinity and wake of the canopy elements. Therefore, the tridimensionality should be limited to high-frequency components of the flow (i.e., turbulence) and should not alter the overall shape of the main vortex. Recent studies have observed that, although in a vegetated urban canyon several factors (aspect ratio, building geometry, surface heating, and tree dimensions and distribution) can modify the circulation, their impacts generally manifest as changes in vortex intensity and position rather than a fundamental breakdown of the bi-dimensional vortex structure. Therefore, we can reasonably use this 2-D theoretical framework to have a first assessment of the circulation regime.

Finally, trees are addressed as aerodynamic obstacles, but their interactions with air pollution include other processes, such as deposition and emission of biogenic volatile organic compounds that can modify the concentration and dispersion of different pollutants (Hu et al., 2016; Simon et al., 2019; Biagi et al., 2025). To partially overcome this issue, we chose carbon monoxide as a benchmark for this analysis since it is a primary pollutant emitted directly from traffic. This limits the emissions from sources other than traffic and the direct chemical interactions with the trees. On the other hand, the present framework does not account for production and destruction caused by inorganic chemical reactions, dry and wet deposition, or reactive chemical pathways within the urban canopy. Trees can modify pollutant concentrations not only aerodynamically but also through deposition processes and the chemical mediation of the production or removal of atmospheric species. CO is less reactive than pollutants such as NO_x or O_3 and is predominantly traffic-emitted, making it suitable for isolating turbulent transport and ventilation effects over the investigated timescales. Nevertheless, some contribution from deposition and indirect chemical transformations cannot be excluded. Therefore, the conclusions of this study should be interpreted primarily in terms of the aerodynamic and turbulent controls exerted by trees on pollutant dispersion and removal, rather than as a complete assessment of all vegetation–air quality interactions.

6. Conclusion

The investigation presented in this paper builds upon the results of Barbano et al. (2021) and the methodological framework of Dallman et al. (2014) to provide an interpretation scheme for air pollutant removal from a street canyon in the presence of vegetation based on turbulent mixing. The scheme comprises two parts: first, trees in the canyon are accounted for as a porous medium with an aerodynamic effect on the flow field and a thermal effect on the canyon surfaces; second, the breathability of the canyon is guided by the vertical transport of momentum and heat, and the mixing thus generated at multiple levels within and above the canopy. The effect of trees has been integrated into the definition of a modified buoyancy parameter B to discern whether the in-canyon circulation is inertially or thermally driven. The efficacy of mixing at different levels of the canyon has been computed through time scales and exchange rates based on mechanical and thermal contributions to estimate the speed and efficacy at which the atmosphere mixes (or exchanges) its properties inwards and outwards the street canyon. By combining the circulation and relative exchange process, a cumulative exchange rate has been adopted to evaluate the removal of a primary traffic pollutant from the street canyon. The testbed for the entire investigation was the street canyon of LB, and the analyses were conducted using experimental data collected during an ad hoc field campaign in 2017.

The results provide clear indications of the performance of air pollution removal from exchange processes, depending on the relative mixing at different canyon levels, background wind directions, and the shadowing effect of trees. Together with the aspect ratio of the canyon and the morphology of the street, trees are found to favour the inertial dynamics and the formation of mechanical turbulence in the canyon, thanks to the flow channelling in the trunk region and the drag exerted by the crown, respectively. Trees also generate suitable conditions for the thermal circulation at the specific time of the day when one side of the street is in the shadow of the crown. On the other hand, the same shadowing effect limits the heat flux within the canyon, increasing the mixing time therein. Therefore, while mechanical turbulence in the canyon drives fast mixing and an efficient rate of momentum exchange with the atmosphere above, the slow thermal mixing inhibits the corresponding exchange rate, lowering its efficacy. This clear distinction between mechanical and thermal exchanges reveals a distinctive factor compared to the non-vegetated canopy, where the wind direction is the major discriminant of the exchange process efficacy (Barbano et al., 2021). Mixing is also found to modulate its efficacy as a function of the wind direction: mechanical exchanges are always efficient with subtle differences upon wind direction; thermal exchanges are instead particularly ineffective under north parallel and partially oblique wind directions. The impact on ventilation is straightforward, with inertial conditions favouring pollutant removal from the canopy and thermal ones favouring stagnation, with parallel and oblique directions being the worst for pollutant accumulation. As the thermodynamics and turbulence activity develop and evolve within the canyon and its interface with the atmosphere above, the pollutant concentrations are continuously modulated (Fig. 16). Turbulence mixing within the canyon proves vital in triggering an effective pollutant removal: a fast heat and momentum transport compared to the upper canyon is mandatory to have efficient mixing. Conversely, when mixing at the surface is slow, the fresh air entrainment at the top of the canyon does not effectively reach the surface, and the decoupling between the upper and lower parts of the canopy favours air and pollutant trapping towards the surface.

In conclusion, the presence of trees in the canyon provides both benefits and disbenefits for air quality, depending on their impact on the local atmospheric conditions. In a counterintuitive way, limiting the shadowing effect of trees without losing their

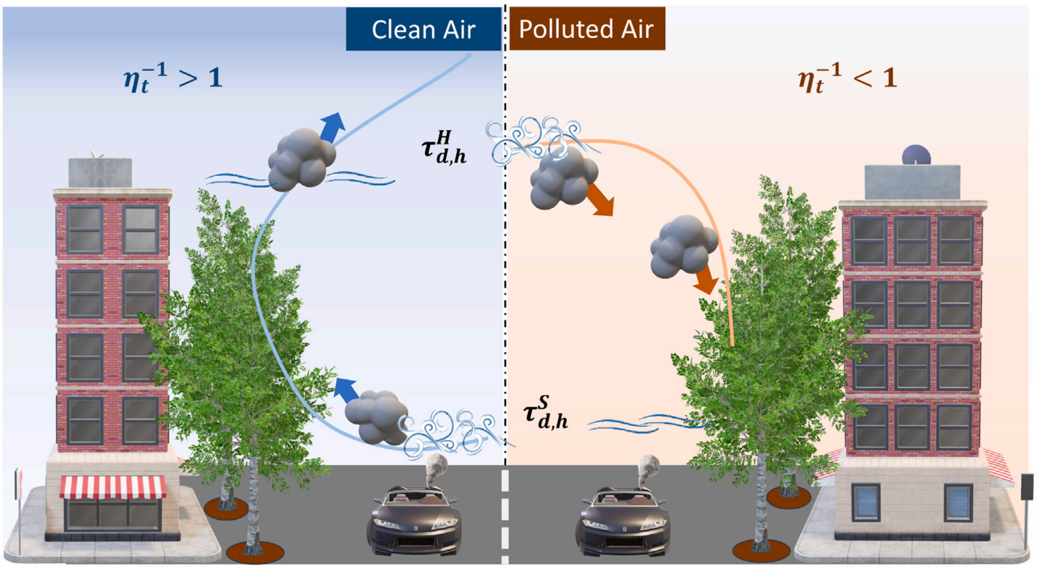

Fig. 16. The intensity of exchange rates η_t^{-1} as ratios of time scales inside the canyon τ^S and at its interface with the atmosphere above τ^H regulates the capability of the canopy circulation and turbulent processes to efficiently remove ($\eta_t^{-1} > 1$ or $\tau^S > \tau^H$) or retain ($\eta_t^{-1} < 1$ or $\tau^S < \tau^H$) the pollutants in the canyon, together with the street morphology (building and vegetation) and shading effects.

dynamic apportionment may facilitate pollutant removal. On the other hand, this solution would reduce the benefits of mitigating local air temperature and thermal comfort. A balance between these aspects must be found to maximise the mitigation our cities can benefit from. Despite providing useful general insights on the role of trees in street canyons and how to address them, this study also highlights the fundamental necessity of conducting ex-ante studies whenever a plantation is planned. A beneficial plantation requires scenario-based assessments of alternative tree arrangements (e.g., varying spacing, crown morphology, or positioning relative to the canyon axis) using computational fluid dynamics (CFD) modelling or wind-tunnel experiments. Such approaches can systematically explore trade-offs between radiative shading (cooling benefits) and aerodynamic effects (ventilation and pollutant dispersion) across different tree configurations, providing urban planners with actionable guidance for implementation. Our study does not provide such a quantitative optimisation, but it highlights the necessity of these ex-ante evaluations.

CRediT authorship contribution statement

Francesco Barbano: Writing – original draft, Visualization, Validation, Software, Methodology, Investigation, Formal analysis, Conceptualization. **Erika Brattich:** Writing – review & editing, Validation, Investigation, Formal analysis, Conceptualization. **Silvana Di Sabatino:** Writing – review & editing, Investigation, Conceptualization.

Declaration of competing interest

The authors declare that they have no known competing financial interests or personal relationships that could have appeared to influence the work reported in this paper.

Acknowledgements

This research has been supported by the iSCAPE (Improving the Smart Control of Air Pollution in Europe) project funded by the European Community's H2020 Programme (H2020-SC5-04-2015) under the Grant Agreement No. 689954 (https://www.iscapeproject.eu/). The authors are pleased to acknowledge all the academics, researchers, specialists, and students from the Department of Physics and Astronomy and the Department of Industrial Engineering of the University of Bologna, the ARPAE, and the National Research Council (CNR) for their tremendous effort dedicated to the realisation of the experimental field campaign. Particularly, we express sincere gratitude to Carla Barbieri and Luca Torreggiani from ARPAE for the deployment and maintenance during the whole period of the instrumentation for air-quality measurements and their active collaboration to realise the experimental design. We also acknowledge Marianna Nardino from CNR for the deployment and installation of part of the instrumentation for the measurement of turbulence. We acknowledge all members of the research group, particularly Beatrice Pulvirenti from the Department of Industrial Engineering of the University of Bologna, Marco Deserti from Regione Emilia–Romagna and Enrico Minguzzi from ARPAE for all the support given during the realisation of the campaign and the fruitful discussions. Special gratitude is given to Massimo Bacchetti (technical support for research at the Department of Physics and Astronomy) for the setting of the station mountings, the field installations and local instrument maintenance during the whole campaign. We sincerely acknowledge the Municipality of Bologna for granting the possibility to deploy the experiments in the city centre, the CGIL (Confederazione Generale Italiana del Lavoro), and private citizens for having hosted part of the instrumentation on private balconies and rooftops. Finally, we acknowledge the suggestions made by three anonymous referees, which have helped us to improve the manuscript substantially.

Appendix 1. Specific settings for thermal imaging

The operational setting of the thermal camera requires a set of parameters to be defined to correctly convert the measure of radiation collected by the instrument into the temperature of the emitting surface and compensate for the ambient conditions and the reflected radiation. The latter are particularly challenging, as the multitude of emitting bodies (other than the subject of your investigation) are additional sources of radiation and reflections that we want to avoid measuring, while the atmosphere can attenuate the signal due to scattering from its compounds. The thermal camera can compensate for both factors thanks to the parameters listed in Table 5, but few precautions were taken: (i) for the detailed investigation, only subjects with high emissivity were chosen, i.e., $\epsilon > 0.9$, to minimise the reflected component from the subject surface; (ii) ambient parameters were constantly monitored to ensure a correct assessment of the atmospheric conditions; (iii) the distance from the subject is minimised to shorten the atmospheric layer the radiation has to travel between the subject and the instrument.

Table 5
Settings of the thermal camera specific for the investigated subjects. ϵ is the emissivity, T_a and T_r are the ambient and reflected temperatures, respectively, and RH_a is the ambient relative humidity, d is the distance between the surface and the instrument. Parameters are equal for the shadowed and non-shadowed surfaces of each subject.

ID	Subject	Time (local)	ϵ	d [m]	T_a [°C]	T_r [°C]	RH_a [%]
IR07b	Building	07:00	0.91	10	20	20	55
IR07s	Street	07:09	0.94	10	20	20	55
IR09b	Building	09:00	0.91	10	23	23	42
IR09s	Street	09:18	0.94	10	25	25	43
IR11b	Building	11:00	0.91	10	31	31	33
IR11s	Street	11:19	0.94	10	32	32	31
IR13b	Building	13:00	0.91	10	31	31	30
IR13s	Street	13:28	0.94	10	31	31	30

Appendix 2. Goodness of fit tests for time scales and exchange rates

The use of the GEV functions to fit time scales τ and exchange rates η distributions at different wind directions is addressed through a set of non-parametric tests and a comparison with other skewed functions. First, the Akaike Information Criterion (AIC) is run on several left-skewed functions, namely exponential, gamma, Weibull, and Generalised Pareto, in addition to the GEV, to identify the optimal function for the data distributions. The test recognises the GEV among the best solutions for every single distribution of τ and η, outperforming the competition or remaining within a delta of AIC smaller than 5 units; the performance of the other functions is instead more erratic, showing large ups and downs depending on the single data distribution. Considering the aggregate performance across all distributions, the GEV achieves the best overall AIC score.

The Kolmogorov–Smirnov (KS) and Anderson–Darling (AD) tests were then used as goodness-of-fit metrics for the GEV functions. Although similar, the first provides a better estimate of the distribution's centre, while the second is more heavily weighted towards the tails. For both tests, the null hypothesis is that each τ and η distribution can be fitted with a GEV function with a significance level of 5% for rejecting it. The p-value is also computed for both tests: for the cases where the null hypothesis is not rejected, it ranges $0.1 \leq p \leq 0.9$ for AD and $0.07 \leq p \leq 0.8$ for KS. Table 6 summarises the results of the tests for each τ and η.

Table 6
Results of the Anderson–Darling (AD) test and the Kolmogorov–Smirnov (KS) test applied on the time scales τ (G = ground level, M = Mid-canyon level, R = Rooftop level) and exchange rates η (GM = Ground/Mid-canyon levels, GR = Ground/Rooftop levels) in LB. The null hypothesis is that τ and η follow a GEV distribution, and we use a 5% significance level to reject it. Tests are run on GEVs computed for the whole period (Overall) and the background wind sectors from Table 3, where NP is north parallel, SP is south parallel, EWP is perpendicular (from east and west), and SW is southwestern. ✓ is inserted when the null hypothesis is not rejected, × when it is rejected.

Level	Overall		NP		SP		EWP		SW	
	AD	KS	AD	KS	AD	KS	AD	KS	AD	KS
τ_d^G	✓	✓	✓	✓	✓	×	✓	✓	✓	✓
τ_d^M	✓	✓	✓	✓	✓	✓	×	×	✓	✓
τ_d^R	✓	✓	✓	✓	✓	✓	✓	×	✓	✓
τ_h^G	✓	✓	✓	×	✓	✓	✓	✓	✓	✓
τ_h^M	✓	✓	✓	✓	✓	✓	×	×	✓	✓
τ_h^R	✓	✓	✓	✓	✓	×	✓	×	✓	✓
η_d^M	✓	✓	✓	✓	✓	×	✓	×	✓	✓
η_d^R	✓	✓	✓	✓	✓	✓	✓	✓	✓	✓
η_h^M	✓	✓	✓	✓	✓	✓	×	×	✓	✓
η_h^R	✓	✓	✓	✓	✓	✓	✓	✓	✓	✓

Data availability

Data will be made available on request.

References

Abhijith, K., Kumar, P., Gallagher, J., McNabola, A., Baldauf, R., Pilla, F., Broderick, B., Di Sabatino, S., Pulvirenti, B., 2017. Air pollution abatement performances of green infrastructure in open road and built-up street canyon environments–A review. Atmos. Environ. 162, 71–86.

Alonso-Estébanez, A., Pascual-Muñoz, P., Yagüe, C., Laina, R., Castro-Fresno, D., 2012. Field experimental study of traffic-induced turbulence on highways. Atmos. Environ. 61, 189–196.

Barbano, F., Brattich, E., Di Sabatino, S., 2021. Characteristic scales for turbulent exchange processes in a real urban canopy. Bound.-Layer Meteorol. 178, 119–142.

Barbano, F., Di Sabatino, S., Stoll, R., Pardyjak, E.R., 2020. A numerical study of the impact of vegetation on mean and turbulence fields in a European-city neighbourhood. Build. Environ. 186, 107293.

Barlow, J.F., Belcher, S.E., 2002. A wind tunnel model for quantifying fluxes in the urban boundary layer. Bound.-Layer Meteorol. 104, 131–150.

Barlow, J.F., Harman, I.N., Belcher, S.E., 2004. Scalar fluxes from urban street canyons. Part I: Laboratory simulation. Bound.-Layer Meteorol. 113, 369–385.

Bentham, T., Britter, R., 2003. Spatially averaged flow within obstacle arrays. Atmos. Environ. 37, 2037–2043.

Biagi, B., Brattich, E., Cintolesi, C., Barbano, F., Di Sabatino, S., 2025. Dynamical and chemical impacts of urban green areas on air pollution in a city environment. Urban Clim. 60, 102343.

Brogno, L., Barbano, F., Leo, L., Di Sabatino, S., 2025. Review on heatwaves: A risk perspective. Environ. Res. Lett. 20, 063004.

Buccolieri, R., Gromke, C., Di Sabatino, S., Ruck, B., 2009. Aerodynamic effects of trees on pollutant concentration in street canyons. Sci. Total Environ. 407, 5247–5256.

Buccolieri, R., Jeanjean, A.P., Gatto, E., Leigh, R.J., 2018. The impact of trees on street ventilation, nox and pm2. 5 concentrations across heights in Marylebone Rd Street Canyon, Central London. Sustain. Cities Soc. 41, 227–241.

Buccolieri, R., Salim, S.M., Leo, L.S., Di Sabatino, S., Chan, A., Ielpo, P., de Gennaro, G., Gromke, C., 2011. Analysis of local scale tree–atmosphere interaction on pollutant concentration in idealized street canyons and application to a real urban junction. Atmos. Environ. 45, 1702–1713.

Buccolieri, R., Sandberg, M., Di Sabatino, S., 2010. City breathability and its link to pollutant concentration distribution within urban-like geometries. Atmos. Environ. 44, 1894–1903.

Cai, C., Ming, T., Fang, W., De Richter, R., Peng, C., 2020. The effect of turbulence induced by different kinds of moving vehicles in street canyons. Sustain. Cities Soc. 54, 102015.

Che, W., Zhuang, W., 2025. Integrated vegetation effects on thermal environment and air quality in urban street canyons. Urban Clim. 63, 102593.

Chen, L., Hang, J., Sandberg, M., Claesson, L., Di Sabatino, S., 2017. The influence of building packing densities on flow adjustment and city breathability in urban-like geometries. Procedia Eng. 198, 758–769.

Cheng, W.C., Liu, C.H., Leung, D.Y.C., 2009. On the correlation of air and pollutant exchange for street canyons in combined wind-buoyancy-driven flow. Atmos. Environ. 43, 3682–3690.

Cintolesi, C., Barbano, F., Di Sabatino, S., 2021. Large-eddy simulation analyses of heated urban canyon facades. Energies 14, 3078.

Cintolesi, C., Barbano, F., Trudu, P.L., Finco, A., Gerosa, G., Di Sabatino, S., 2023. Characterisation of flow dynamics within and around an isolated forest, through measurements and numerical simulations. Agricult. Forest. Meterol. 339, 109557.

Cui, D., Zhou, T., Liang, G., Fan, Y., Mak, C.M., 2026. Numerical study on natural-ventilated pollutant transportation in street canyons with green infrastructure under vegetation-induced thermal conditions. Urban Clim. 66, 102833.

Dallman, A., Magnusson, S., Britter, R., Norford, L., Entekhabi, D., Fernando, H.J.S., 2014. Conditions for thermal circulation in urban street canyons. Build Env. 80, 184–191.

Del Ponte, A.V., Fellini, S., Marro, M., Soulhac, L., Ridolfi, L., Salizzoni, P., 2025. The turbulent flow within a wind-aligned street canyon with trees: An experimental study. Bound.-Layer Meteorol. 191, 21.

Del Ponte, A.V., Fellini, S., Marro, M., van Reeuwijk, M., Ridolfi, L., Salizzoni, P., 2024. Influence of street trees on turbulent fluctuations and transport processes in an urban canyon: A wind tunnel study. Bound.-Layer Meteorol. 190, 6.

Deng, J.Y., Wong, N.H., 2020. Impact of urban canyon geometries on outdoor thermal comfort in central business districts. Sustain. Cities Soc. 53, 101966.

Di Nicola, F., Brattich, E., Di Sabatino, S., 2022. A new approach for roughness representation within urban dispersion models. Atmos. Environ. 283, 119181.

Di Sabatino, S., Barbano, F., Brattich, E., Pulvirenti, B., 2020. The multiple-scale nature of urban heat island and its footprint on air quality in real urban environment. Atmosphere 11, 1186.

Di Sabatino, S., Buccolieri, R., Pappaccogli, G., Leo, L.S., 2015. The effects of trees on micrometeorology in a real street canyon: Consequences for local air quality. Int. J. Environ. Pollut. 58, 100–111.

Di Sabatino, S., Kastner-Klein, P., Berkowicz, R., Britter, R., Fedorovich, E., 2003. The modelling of turbulence from traffic in urban dispersion models—part I: Theoretical considerations. Environ. Fluid Mech. 3, 129–143.

European Environment Agency, 2016. EMEP/EEA Air Pollutant Emissions Inventory Guidebook 2016: Technical Guidance to Prepare National Emission Inventories. EEA Report No 21/2016.

Fellini, S., Marro, M., Del Ponte, A.V., Barulli, M., Soulhac, L., Ridolfi, L., Salizzoni, P., 2022. High resolution wind-tunnel investigation about the effect of street trees on pollutant concentration and street canyon ventilation. Build. Environ. 226, 109763.

Giometto, M.G., Christen, A., Egli, P.E., Schmid, M.F., Tooke, R., Coops, N., Parlange, M.B., 2017. Effects of trees on mean wind, turbulence and momentum exchange within and above a real urban environment. Adv. Water Resour. 106, 154–168.

Goncalves, R., Linhares, C., Yojo, T., 2023. Drag coefficient in urban trees. Trees 37, 133–145.

Gordon, M., Staebler, R.M., Liggio, J., Makar, P., Li, S.M., Wentzell, J., Lu, G., Lee, P., Brook, J.R., 2012. Measurements of enhanced turbulent mixing near highways. J. Appl. Meteorol. Clim. 51, 1618–1632.

Gromke, C., Buccolieri, R., Di Sabatino, S., Ruck, B., 2008. Dispersion study in a street canyon with tree planting by means of wind tunnel and numerical investigations–evaluation of CFD data with experimental data. Atmos. Environ. 42, 8640–8650.

Hankey, S., Marshall, J.D., 2017. Urban form, air pollution, and health. Curr. Environ. Health Rep. 4, 491–503.

Harman, I.N., Barlow, J.F., Belcher, S.E., 2004. Scalar fluxes from urban street canyons part II: Model. Bound.-Layer Meteorol. 113, 387–410.

Højstrup, J., 1993. Statistical data screening procedure. Meas. Sci. Technol. 4, 153–157.

Hu, Y., Zhao, P., Niu, J., Sun, Z., Zhu, L., Ni, G., 2016. Canopy stomatal uptake of nox, so2 and o3 by mature urban plantations based on sap flow measurement. Atmos. Environ. 125, 165–177.

Jeanjean, A.P., Hinchliffe, G., McMullan, W., Monks, P.S., Leigh, R.J., 2015. A CFD study on the effectiveness of trees to disperse road traffic emissions at a city scale. Atmos. Environ. 120, 1–14.

Kampa, M., Castanas, E., 2008. Human health effects of air pollution. Environ. Pollut. 151, 362–367.

Kastner-Klein, P., Berkowicz, R., Britter, R., 2004. The influence of street architecture on flow and dispersion in street canyons. Meteorol. Atmos. Phys. 87, 121–131.

Kastner-Klein, P., Rotach, M.W., 2004. Mean flow and turbulence characterisitcs in a urban roughness sublayer. Bound.-Layer Meteorol. 111, 55–84.

Kim, J.J., Baik, J.J., 2003. Effects of inflow turbulence intensity on flow and pollutant dispersion in an urban street canyon. J. Wind Eng. Ind. Aerodyn. 91, 309–329.

Klein, P.M., Galvez, J.M., 2015. Flow and turbulence characteristics in a suburban street canyon. Env. Fluid Mech. 15, 419–438.

Lalic, B., Mihailovic, D.T., 2004. An empirical relation describing leaf-area density inside the forest for environmental modeling. J. Appl. Meteorol. 43, 641–645.

Li, X.X., Britter, R.E., Norford, L.K., Koh, T.Y., Entekhabi, D., 2012. Flow and pollutant transport in urban street canyons of different aspect ratios with ground heating: Large-eddy simulation. Bound.-Layer Meteorol. 142, 289–304.

Li, R., Niu, J., Zhao, Y., Wang, L.L., Shi, X., Gao, N., 2025. Wind tunnel experiments on the aerodynamic effects of a single potted tree: Hot-wire anemometry and piv measurements. Urban Clim. 62, 102520.
Liu, C.H., Leung, D.Y.C., Barth, M.C., 2005. On the prediction of air and pollutant exchange rates in street canyons of different aspect ratios using large-eddy simulation. Atmos. Environ. 39, 1567–1574.
Livesley, S., McPherson, E.G., Calfapietra, C., 2016. The urban forest and ecosystem services: Impacts on urban water, heat, and pollution cycles at the tree, street, and city scale. J. Environ. Qual. 45, 119–124.
Lo, K.W., Ngan, K., 2017. Characterizing ventilation and exposure in street canyons using Lagrangian particles. J. Appl. Meteorol. Clim. 56, 1177–1194.
Louka, P., Belcher, S., Harrison, R., 1998. Modified street canyon flow. J. Wind Eng. Ind. Aerodyn. 74, 485–493.
McMillen, R.T., 1988. An eddy correlation technique with extended applicability to non-simple terrain. Bound.-Layer Meteorol. 43, 231–245.
Miri, A., Webb, N.P., 2022. Characterizing the spatial variations of wind velocity and turbulence intensity around a single tamarix tree. Geomorphology 414, 108382.
Moayedi, S.H., Hassanzadeh, S., 2022. An les study of aerodynamic effect of trees on traffic pollutant dispersion in an ideal street canyon. Eur. Phys. J. Plus 137, 797.
Murena, F., Favale, G., 2007. Continuous monitoring of carbon monoxide in a deep street canyon. Atmos. Environ.
Nazarian, N., Martilli, A., Kleissl, J., 2017. Impacts of realistic urban heating, part I: Spatial variability of mean flow, turbulent exchange and pollutant dispersion. Bound.-Layer Meteorol. 166, 367–393.
Nazarian, N., Martilli, A., Norford, L., Kleissl, J., 2018. Impacts of realistic urban heating. Part II: Air quality and city breathability. Bound.-Layer Meteorol. 168, 321–341.
Nelson, M.A., Pardyjak, E.R., Brown, M.J., Klewicki, J.C., 2007. Properties of the wind field within the oklahoma city park avenue street canyon. Part II: Spectra, cospectra, and quadrant analyses. J. Appl. Meteorol. Clim. 46, 2055–2073.
Nosek, Š., Kukačka, L., Kellnerová, R., Jurčáková, K., Jaňour, Z., 2016. Ventilation processes in a three-dimensional street canyon. Bound.-Layer Meteorol. 159, 259–284.
Oke, T., 1987. Boundary Layer Climates, second ed. Routledge, Methuen, UK.
Perez, D.M., Canfield, J.M., Linn, R.R., Speer, K., 2025. Characterizing turbulence at a forest edge: A vorticity budget analysis around a canopy. Agricult. Forest. Meterol. 363, 110422.
Piracha, A., Chaudhary, M.T., 2022. Urban air pollution, urban heat island and human health: A review of the literature. Sustainability 14, 9234.
Pope, S.B., 2001. Turbulent flows. Meas. Sci. Technol. 12, 2020–2021.
Rao, S.T., Sedefian, L., Czapski, U.H., 1979. Characteristics of turbulence and dispersion of pollutants near major highways. J. Appl. Meteorol. Clim. 18, 283–293.
Salizzoni, P., Marro, M., Soulhac, L., Grosjean, N., Perkins, R.J., 2011. Turbulent transfer between street canyons and the overlying atmospheric boundary layer. Bound.-Layer Meteorol. 141, 393–414.
Salmond, J.A., Tadaki, M., Vardoulakis, S., Arbuthnott, K., Coutts, A., Demuzere, M., Dirks, K.N., Heaviside, C., Lim, S., Macintyre, H., et al., 2016. Health and climate related ecosystem services provided by street trees in the urban environment. Environ. Health 15, S36.
Santiago, J.L., Buccolieri, R., Rivas, E., Sanchez, B., Martilli, A., Gatto, E., Martín, F., 2019. On the impact of trees on ventilation in a real street in Pamplona, Spain. Atmosphere 10, 697.
Schmid, H.P., Grimmond, C.S.B., Cropley, F., Offerle, B., Su, H.B., 2000. Measurements of CO2 and energy fluxes over a mixed hardwood forest in the mid-western united states. Agric. Meteorol. 103, 357–374.
Simon, H., Fallmann, J., Kropp, T., Tost, H., Bruse, M., 2019. Urban trees and their impact on local ozone concentration–A microclimate modeling study. Atmosphere 10, 154.
Solazzo, E., Britter, R.E., 2007. Transfer processes in a simulated urban street canyon. Bound.-Layer Meteorol. 124, 43–60.
Soulhac, L., Perkins, R.J., Salizzoni, P., 2008. Flow in a street canyon for any external wind direction. Bound.-Layer Meteorol. 126, 365–388.
Ullah, M.S., Di Giulio, A., Cintolesi, C., Di Sabatino, S., 2025. Assessing the influence of rooftop vegetation on pollution dispersion in urban canyons through large-eddy simulations. Urban Clim. 64, 102614.
Vickers, D., Mahrt, L., 1997. Quality control and flux sampling problems for tower and aircraft data. J. Atmos. Ocean. Technol. 14, 512–526.
Zajic, D., Fernando, H., Calhoun, R., Princevac, M., Brown, M.J., Pardyjak, E., 2011. Flow and turbulence in an urban canyon. J. Appl. Meteorol. Clim. 50, 203–223.
Zhang, B., Ooka, R., Kikumoto, H., 2022a. Spatiotemporal spectral analysis of turbulent structures and pollutant removal in two-dimensional street canyon. Bound.-Layer Meteorol. 185, 63–91.
Zhang, B., Ooka, R., Kikumoto, H., 2022b. Spectral proper orthogonal decomposition analysis of turbulent flow in a two-dimensional street canyon and its role in pollutant removal. Bound.-Layer Meteorol. 183, 97–123.
Zhao, Y., Li, H., Bardhan, R., Kubilay, A., Li, Q., Carmeliet, J., 2023. The time-evolving impact of tree size on nighttime street canyon microclimate: Wind tunnel modeling of aerodynamic effects and heat removal. Urban Clim. 49, 101528.